MICROWAVE PYROLYSIS BIOCHAR CHARACTERIZATION AND MODELING OF CHAR REINFORCED GFRP BIOCOMPOSITES

by

Chase A. Wallace

B.Sc. Mechanical Engineering, University of New Brunswick, 2017

A Thesis Submitted in Partial Fulfillment
of the Requirements for the Degree of

Master of Science in Engineering

in the Graduate Academic Unit of Mechanical Engineering

Co-Supervisors: Gobinda C. Saha, PhD, UNB Mechanical Engineering

Muhammad T. Afzal, PhD, UNB Mechanical Engineering

Examining Board: Tiger Jeans, PhD, UNB Mechanical Engineering (Chair)

Clodualdo Jr. Aranas, PhD, UNB Mechanical Engineering

Rickey Dubay, PhD, UNB Mechanical Engineering

Huining Xiao, PhD, UNB Chemical Engineering (External)

This thesis is accepted by the
Dean of Graduate Studies

THE UNIVERSITY OF NEW BRUNSWICK

April, 2019

ABSTRACT

This research thesis focuses on the manufacturing and characterization of biochar synthesized from microwave pyrolysis, as well as the manufacturing, testing, and modelling of a novel three-part biocomposites through the addition of biochar as a reinforcing filler to the common glass-fiber reinforced polymer (GFRP) composite. Biochar was produced from both softwood and hemp feedstocks utilizing a large batch of one kilogram of biomass mixed with 10 wt.% of microwave absorber, pyrolyzed at a constant residence time of 1 hour. The microwave power levels of 2100, 2400, and 2700 Watts were selected after several preliminary trials. Pyrolysis heating rates for large batch of biomass loading was found ranging from 25-50 ^{o}C/min. A number of characterization techniques were employed for the biochars including physiosorption analysis, proximate/ultimate analysis, FT-IR spectroscopy, and nanoindentation. Overall characteristics were improved through increasing microwave powers during pyrolysis.

Biocomposites were produced in-house through a pultrusion process, and varying the biochar matrix volume percentage by 5, 10, and 20%. Through mechanical testing, the addition of biochar was found to increase the flexural yield strength and modulus of the biocomposites to a maximum of 34 and 6.5% respectively at 20% hemp biochar loading. Tensile testing revealed that the addition of biochar had some influence on tensile properties of the biocomposites, with maximum tensile strength and modulus increases being 12.5 and 2.6% respectively. Rule of mixtures and homogenization micromechanical models were evaluated against the experimental results to determine their validity for these novel three-part biocomposites, with

the largest percent difference being 13%. A finite element model was created and analyzed through Abaqus FEA software for homogenization modeling.

DEDICATION

To my wonderful parents Gary and Keitha, who provide limitless support and encouragement towards their son. He wishes to truly express the love and admiration he feels back.

To Shea, my very own honeybee.

And to my friends who continue to motivate and elevate each other throughout the years.

ACKNOWLEDGEMENTS

I would first like to acknowledge and express my sincere gratitude to my academic co-supervisors Dr. Gobinda C. Saha and Dr. Muhammad T. Afzal, who have provided guidance and support throughout my time here at the University of New Brunswick. Their patience and motivation has been the driving factor in my success and a great influence in the academic I strive to be. I am so very grateful for the countless opportunities you both have provided me.

I would also like to acknowledge the many people and groups that helped provide support throughout the experimental testing of this thesis. The physiosorption analysis and FT-IR work was supported by Cape Breton University. The SEM imaging was carried out with the help of Steven Cogswell at UNB's Microscopy and Microanalysis Facility (MMF). Andrew Sutherland (UNB, Civil Engineering) and Vince Boardman (UNB, Mechanical Engineering) both provided extensive guidance and support throughout the mechanical testing phase. Dr. Alan Lloyd also lent his extensive knowledge of mechanical testing and assisted in digital image correlation. I would also like to thank the number of undergraduate students who helped perform pyrolysis experiments.

Finally, this thesis would not have been possible without the financial support of the Natural Sciences and Engineering Research Council of Canada (NSERC), New Brunswick Innovation Foundation (NBIF), and New Brunswick Department of Agriculture, Aquaculture and Fisheries (NBDAAF).

Table of Contents

List of Tables

List of Figures

Chapter 2: Literature Review

Chapter 3: Methodology

Chapter 4: Current Progress and Results

Appendix

Chapter 1

Introduction

1.1 Motivation

Sustainability has been a common theme driving research and industry in recent years as we become more aware and sensitive to the changing global environment. Sustainable energy, fuels, and materials are becoming important research sectors as we strive to maintain our current levels of global infrastructure without further harming the environment. One sustainable approach is the thermochemical conversion of waste biomass to produce biofuels and bio-products.

Biomass pyrolysis is a thermal conversion process in the absence of oxygen to produce gaseous and aqueous bio-products as well as biochar residues [1]. Biochar is known to be a renewable solid consisting of a porous honeycomb structure which gives it a high specific surface area. Due to the unique structure of this carbon-based material, it is typically used in carbon sequestration, soil remediation, and filtration. Recent research has considered another use of biochar, as a renewable filler material in biocomposites materials. The driving factors for the potential of these sustainable materials are that they must have compatible characteristics or performance properties in order to potentially replace their synthetic or inorganic counterparts [2].

Only recently has research introduced the idea of biochar as a particle reinforcing filler to epoxy, and wood-laminate composite materials [3]. The studies report a favorable increase in flexural and tensile mechanical properties owing to addition of biochar causing a reinforcing effect due to the particle hardness and mechanical interlocking with the polypropylene matrix [3, 4]. These findings indicate that a highly porous, high specific surface area, biochar of large carbon content would be favorable in the development of biocomposites materials.

Conventional pyrolysis is a direct heating method, in which biomass feedstock is heated through conduction or convection from hot solid or gas transfer media. Lately research interest has turned to microwave pyrolysis due to the benefits of faster heating rates, selective heating, volumetric and uniform heating which leads to a faster process and less energy consumption. These benefits are gained from the dielectric microwave heating method in which the polar molecules of the biomass continually try to rotate and align with the electric wave frequency, causing heat from the friction and collisions of the rotations. This non-contact energy transfer process from electric to thermal energy is much faster than the conventional pyrolysis process in which thermal energy must overcome the heat transfer barrier of conduction or convection [5]. Further cited benefits of microwave pyrolysis is the instantaneous start-up/shut down of the process leading to better control over the time, temperature, and energy consumption process parameters [6, 7].

Comparing biochar from conventional and microwave pyrolysis, recent studies have found that both the surface area and pore volume are significantly higher for microwave-

pyrolysis-biochar, attributed to a more rapid free release of volatiles during the faster-heating-rate process [8]. Biochar with these increased structural characteristics is found to be of use in the development of sustainable biocomposites materials.

This research study uses the microwave pyrolysis process to create large batches of highly porous, high specific surface area biochar which is introduced as a particulate filler in common glass-fiber reinforced polymer rebar. Through the use of multiple feedstocks, testing parameters, and characterization techniques, valuable insight is found on the potential of this novel biocomposites material.

1.2 Objectives

This study further develops the concept and understanding of microwave-pyrolysis-biochar as a particulate filler in glass-fiber reinforced composites. The following objectives were developed in order to understand the scope of work:

1. Manufacture biochar under optimized process parameters at varying power levels
2. Identify mechanical/chemical characteristics of biochar
3. Manufacture quality GFRP/Biochar – biocomposites material through the use of a pultrusion machine
4. Utilize analytical micromechanical models describing biocomposites effective elastic coefficients through rule of mixtures, and homogenization methods
5. Test mechanical properties of novel biocomposites and compare to the analytical model

Chapter 2

Literature Review

2.1 Background Concepts

2.1.1 Thermochemical Conversions

Thermochemical conversions are the process of converting biomass to its base constituents using heat. Biomass is considered to be any organic material that can decompose, this includes all carbonaceous plant and animal matter. The main thermochemical processes are torrefaction, pyrolysis, gasification, and combustion. Torrefaction involves heating of biomass at lower temperatures (200-300°C) in the absence of oxygen. The main use of this mild heat treatment is to improve biomass properties prior to further conversion. There properties include: energy density, bulk density, and moisture reduction. Similar to torrefaction, the pyrolysis procedure occurs in the absence of oxygen, but at much higher temperatures (300-1000°C). The end products of pyrolysis are bio-oil, biochar, and synth-gas. Finally gasification occurs at elevated temperatures to pyrolysis (800-1200°C) during with the presence of deficient amounts of oxygen in order to produce higher synth-gas yields [1].

2.1.2 Microwave Pyrolysis

Microwave pyrolysis has recently been gaining in research popularity due to its advantages over conventional pyrolysis. Conventional pyrolysis utilizes traditional heat transfer forms of conduction or convection which is a slower process, taking some time to travel through

the biomass and heat the entire feedstock. Microwave heating is considered a faster process due to the nature of the heating mechanism. The electric field of microwave heating causes polar molecules to rotate, trying to align, the rotation and movement causes increased friction and collision resulting in heat loss of the dipoles causing microwave heating to the biomass. Comparing the two heating mechanisms between conventional and microwave pyrolysis, it is noted that microwave heating is a significantly more controllable process. The electric nature of microwave heating offers a rapid and convenient start-up and shutdown as well as instantaneous heating, proving to hold better process and parameter (time, temperature, power) control over conventional heating. Although microwave heating can be considered a faster process, the process is highly dependent on the rate of microwave absorption in the feedstock. Dry biomass is prone to poor microwave absorption due to lack of moisture, to increase the absorption rate microwave absorbers are often added to the feedstock which increases the heating rate. Overall the increased heating rate allows for a reduced microwave power requirement needed to reach pyrolysis temperatures. Many different materials can be used as microwave absorbers. The chemical structure, shape, and size of microwave absorbers determine the absorbency [5, 7-9].

2.1.3 Composite Materials

A composite material is typically a manufactured material system containing two or more phases, designed to hold mechanical performance properties that are superior to the independent base materials. The properties of each composite varies depending on the properties of the constituents, the geometry, and distribution of each phase material. Phases generally consist of a matrix material and one or more filling or fiber materials. The

composite material is generally described based on the number of its phases or constituents, such as single phase, two-phase, three phase or multi-phase. Generally two-phase materials are classified by the filler material. The three broad classification categories are particulate filler, discontinuous fibers, and continuous fibers. Each of these categories can be further expanded based on the fiber/particulate direction or orientation [10]. The base material worked with in this study is a two-phase unidirectional continuous fiber-reinforced composite.

Continuous fiber-reinforced composites are known to contain fibers that are much longer than the composite materials cross-sectional width. The mechanical properties of these composites are independent of the fiber length and they are stronger and stiffer than short fiber composites. Typically reinforcing fibers are used due to their high tensile strength, stiffness, density, ease of fabrication and cost of production. The reinforcing fibers used in this study are E-glass fibers which also exhibit high-strength-to-weight ratio and typical glass hardness. Particle reinforced composites consist of particulates of different shapes (spheres, flakes) randomly distributed and embedded within the material matrix. The particle dimensions are typically equal sized and equally dispersed, causing the composite to be considered isentropic. Mechanical properties of these composites are typically weaker than fiber-reinforced due to the smaller size. In this study, biochar is used as a particle-reinforcement. The matrix component of a composite maintains the structural shape and reinforcement alignment while also acting as a stress transfer medium and primary contributor to the materials shear strength and crack resistance. The matrix used in this study is a thermoset polymeric resin. The thermoset undergoes an irreversible chemical

change upon heat treatment known as curing. During the curing process polymers in the resin develop a network structure through crosslinking. These resins known to have low melt viscosity, good fiber impregnation and low process temperatures [11].

Recent trends in composite material research has looked towards our renewable resources as sources for eco-friendly biocomposites. Biochar which typically exhibits high values of particle hardness, stiffness, and surface area, has been considered a sustainable filler for biocomposites due to its superior mechanical properties. Plastic-biochar composites have been manufactured and studied through injection molding. Epoxy-biochar and rubber-biochar composites have also been attempted, and finally recent studies have attempted laminated wood plastic and biochar composites. Many of these studies have shown promise in biocomposites mechanical property enhancement when using biochar as a particulate filler [3, 12].

2.2 Microwave Pyrolysis

2.2.1 Heating Rates

Heating rate of a procedure can vastly change the characteristic results of biochar, certain temperatures also need to be reached in order to guarantee full pyrolysis of the feedstock. The following research articles describe change in heating rates and peak temperatures as they pertain to microwave power levels in pyrolysis experiments.

Huang et al. [13] studied the power level effect on the heating rate of microwave pyrolysis of rice straw. For their experiments rice straw was placed in a quartz crucible directly in

the path of microwaves at various power levels (50-500 W) the heating rate and peak temperatures were recorded and each test was done twice to ensure average results. The results showed that maximum temperature per power level had a fairly linear relationship (250 °C at 200 W, 360 °C at 300 W, 550 °C at 500 W) while maximum heating rate versus power level was an exponential function (80°C/min at 200 W, 100°C/min at 300 W, 500°C/min at 500 W). The separate curve relationships show that at higher power levels, higher temperature can be reached faster due to the higher heating rate, allowing for shorter procedure times. It was noted that there is also a critical power level affected by reactor type and sample size, with lower than critical level power causing low heat performance. For this study the critical power level was found to be 400 watts.

Huang et al. [14] performed further research on heating performance from studying seven agricultural feedstocks under microwave pyrolysis. The seven lignocellulosic feedstocks used were bamboo leaves, rice straw, rice husk, corn stover, sugarcane bagasse, sugarcane peel, and coffee grounds. Each feedstock was shredded/sieved and 3-5 grams underwent microwave pyrolysis at the designated power level (300-500W) for 30 minutes. The resulting temperature profiles show that each experiment had various heating rates and maximum temperature but all reached peak temperatures within the first 15 minutes, plateauing for the remainder of the experiment. The resulting data from 300, 400, 500 Watt power levels give heating values of 51-69, 76-103, 98-140°C/min respectively, as well as max temperatures of 346-406, 439-503, and 478-551°C. The data gathered by this study indicates that higher microwave power levels lead to higher heating rates and maximum temperatures.

Liu et al. [15] analyzed heating rates during microwave pyrolysis using tobacco stem as a feedstock. The experiments was completed using 15 grams of crushed tobacco stem at power levels from 400 to 700 watts. For these experiments no catalyst was used as a microwave absorber, and a standard thermocouple was using to record temperatures in real time. The resulting heating rates of 0.316, 0.471, 1.760, and 4.005°C/s were shown to rise with the rising power levels 400, 500, 600, and 700 W respectively. The maximum temperatures reached were 191, 316, 600, and 900°C. This information aligns with other studies stating that a rise in power level will give an increase in heating rate and maximum temperatures. Of note during this study is the difference in temperature profiles due to power level. It was found that at 400 and 500 watts, the temperature profile showed a slow rise followed by a steady balance, while at 600 and 700 watts, the profile consisted of a slow rise followed by a rapid climb and then a steady balance.

The three published journal articles reviewed for this section all agree that higher microwave power levels lead to higher heating rates and higher maximum temperatures. It is important to monitor the temperature profiles in order to reach acceptable pyrolysis levels without excessive power levels in order to be energy efficient. The information found in these articles will serve as good bench marks when scaling the expected power levels and heating rates to our microwave reactor size.

2.2.2 Yield Studies

As power levels change heating rates and maximum temperatures of the pyrolysis process, temperature rises also affect the yield of each constituent of the pyrolysis process. The following experimental research articles give some insight of how different power levels or temperatures will affect the end yield of microwave pyrolysis.

Zhao et al. [16] conducted a study detailing the effects of temperature on the yields of products from microwave pyrolysis of wheat straw. The experiments performed utilized microwave pyrolysis on 10 grams of dried wheat straw mixed with 5 grams of residue biochar as a microwave absorber. The experiments were done on a temperature controlled system for 10 minutes after the reaction temperatures (400, 500, 600°C) were met. Each experiment was completed twice to get an average result. From collection and measurement of the resulting biochar after the experiment, the yield percentages were found. The results show that as temperatures increase from 400 – 500°C the yield of biochar decreased from 57.1 – 47.8%. When increasing from 500 – 600°C the biochar yield hardly changed, decreasing from 47.8 – 47.0% These results indicate that lower temperatures are favorable for increased char yields, while past a certain temperature, the char yield may not be affected anymore.

Yu et al. [17] published research in which they studied microwave pyrolysis of corn cob. Experiments were conducted using 150 grams of dried and ground corn cob in a quartz glass flask inside a microwave reactor. The reactor was temperature controlled with 300, 450, and 600°C used for each batch. Each experiment was conducted for 60 minutes and a

total of four times to achieve an average. Collecting and measuring the amount of biochar after each run gave insight to the effect of reaction temperature on char yield. Resulting averaged data showed that at 300°C, biochar yield was about 65% while yield dropped to 25 and 20% at 450 and 600°C respectively. This information indicates that as reaction temperatures increase, biochar yield will decrease. Also, the difference in char yield at higher temperatures becomes less as more volatile mass has already been released during temperature rise.

Hossain et al. [18] researched the use and benefits of microwave pyrolysis of oil palm fiber for biochar production. Each test was ran using 30 grams of dried oil palm fiber in a quartz tube microwave reactor for 15 minutes with or without a catalyst. Tests were ran in 100 watt increments from 400-900 watts, and each test was ran three times to gain an average. Weighing the resulting biochar after each test and dividing it by the original feedstock weight gave the total biochar yield percentage for each test. The results for tests without a microwave absorbing catalyst show that at 400 watts the biochar yield was 28%, at 600 watts biochar yield was 25%, and at 800 watts biochar yield was 18%. These results show that as power level increases, the expected biochar yield should decrease. Of note is the small percentage change from 400 – 600 watts (3%) followed by the large percentage change between 600 – 800 watts (7%), this data indicates that at lower power levels similar amounts of volatiles are released from the feedstock, and that there is a power or temperature threshold that must be surpassed for much more volatiles to be released.

Each of the three research articles examined on the yield of biochar from microwave pyrolysis detail similar findings. As power level or process temperature increase the percentage yield of biochar decreases. The difference in char yields between higher process temperatures is typically small. Overall, the results indicate that lower temperatures are favorable for high biochar yields. The results of these studies will be considered as power levels are chosen for this study.

2.3 Biochar Characterization

2.3.1 Chemical and Porosity

Chemical and Porosity characterization of biochar is necessary to determine the quality of the char. A high quality char is typically thought to have higher carbon content and higher specific surface area due to its value in filtration and soils amendment. The following studies all detail the characterization results of microwave pyrolysis of various feedstocks at different power levels.

Mohamed et al. [19] used increasing weights of microwave absorbers (clinoptilolite, K_3PO_4) during their research on the microwave pyrolysis process of switchgrass. Considering switchgrass has low microwave absorbency, the authors were interested in the effects of using microwave absorbers to increase heating rates of the process. The experiments were conducted at 750 watts for approximately 30 minutes. The three weight percentages of catalysts were 10, 20 and 30% and each test was done three times in order to get an average. The resulting biochar was tested using a Perkin-Elmer 2400Series II

CHNS/O analyzer to determine the heating rate effects on chemical composition, the results of which are given in Table 2.3.1.1.

Table 2.3.1.1: Elemental composition of biochar produced with various absorber loadings [19]

Biochar type	10 wt.% Clinoptilolite	30 wt.% Clinoptilolite	10 wt.% K_3PO_4	30 wt.% K_3PO_4
Elemental composition (wt.%)[a]				
C	57.31	35.83	42.88	25.86
H	0.38	0.10	0.36	1.39
N	1.10	0.82	0.54	0.31
O[b]	12.24	14.62	20.41	12.76
Ash (wt.%)[a]	28.97	48.63	35.81	59.68

The resulting biochar was put through BET testing to determine the surface area and BJT testing to find the micropore volume. The results showed that increasing clinoptilolite amounts from 10 to 30% increased the heating rate by 40°C/min while increasing the SSA by 13.82 m^2/g, while increasing K_3PO_4 amounts from 10 to 30% did not increase the heating rate, and changes in SSA were negligible. It should be noted that at 20% K_3PO_4 weight the heating rate increased by 34°C/min and SSA by 19.82 m^2/g. A full list of results is given in Table 2.3.1.2

Table 2.3.1.2: Porosity properties of biochar produced with various absorber loadings [19]

Biochar type	BET surface area (m^2/g)	Average diameter (nm)	Micropore area (m^2/g)	Pore volume (cm^3/g)
10 wt.% Clinoptilolite	33.11	2.15	10.89	0.0091
20 wt.% Clinoptilolite	34.06	2.43	14.68	0.0107
30 wt.% Clinoptilolite	46.93	2.22	26.76	0.0141
10 wt.% K_3PO_4	33.51	2.15	20.12	0.0107
20 wt.% K_3PO_4	53.33	2.11	37.92	0.0275
30 wt.% K_3PO_4	39.21	2.19	24.33	0.0128

Zhu et al. [20] conducted research detailing characterization results from microwave-assisted pyrolysis of corn stover. The experiments were performed using a 700 watt microwave. A 500ml quartz flask inside the microwave contained the biomass, while a dead end quartz tube reaching the center of the flask contained an infrared temperature sensor. Experiments were ran at a temperature range from 500-680°C by heating the biomass to the desired temperature at maximum power then lowering the power to maintain that temperature for the desired time. Table 2.3.1.3 details the chemical composition results from testing of biochar produced at 550°C compared to biochar at 650°C. It is noted that the carbon weight percentage raises by approximately 13% with just a 100°C heat rise. As shown in Table 2.3.1.4; three runs of biochar were analyzed using BET surface area techniques to determine the specific surface area (m^2/g) and other porosity factors (average pore volume/width). It is noted that at increasing temperatures and operation times the BET surface area vastly increases, while average pore volume also increases.

Table 2.3.1.3: Elemental composition of biochar produced at separate temperatures [20]

Characteristics	Biochar – 550 °C	Biochar – 650 °C
Elemental analysis (wt.%)		
C	68.01	81.47
H	1.84	0.72
N	0.74	0.69
O	5.94	4.38
S	0.05	0.04
O/C molar ratio	0.12	0.07
H/C molar ratio	0.32	0.11
Ash (wt.%)	23.42	12.70

Table 2.3.1.4: Porosity properties of biochar produced under separate conditions [20]

Run	Conditions	BET surface area (m^2/g)	Average pore volume (cm^2/g)	Average pore width (nm)
3	550 °C, 10 min	9.1	0.009	14.7
5	550 °C, 20 min	18.3	0.011	8.7
15	600 °C, 15 min	45	0.021	6.6

Zhao et al. [21] analyzed shredded wheat straw as a feedstock for production of microwave pyrolysis biochar. The research was conducted using 30grams of shredded wheat straw as the biomass feedstock for microwave pyrolysis experiments at varying temperatures. The resulting biochar was analyzed using the multi-point Brunauer, Emmett, and Teller (BET) method to determine the specific surface area and porosity characteristics. Table 2.3.1.5 details the results at a range of temperatures from 400 to 600 °C. It is noted that SSA (m^2/g) and pore volume (cm^3/g) increase with a rise in residence temperature while average pore size (Å) reduces. This indicates that a larger number of volatiles were released with increasing temperatures, causing a larger number of small pores to open, giving the biochar a more uniform porosity. The main chemical elements of the resulting biochar were also measured using an elemental analyzer. The results tabulated in Table 2.3.1.6 show that as process temperature rises weight percentages of carbon and sulphur slowly increase while the weight percentages of the other three elements reduce.

Table 2.3.1.5: Porosity properties of wheat straw biochar produced at varying temperatures [21]

Temperature (°C)	S_{BET} (m^2/g)	V_T (cm^3/g)	d_{ave} (Å)
400	0.89	0.006	282.16
500	3.33	0.010	118.59
600	9.81	0.012	46.64

Table 2.3.1.6: Elemental composition of wheat straw biochar produced at varying temperatures [21]

Temperature (°C)	C	H	O[a]	N	S
400	52.18	2.79	37.30	1.06	0.77
500	53.01	2.49	36.26	0.94	1.40
600	53.67	2.34	35.49	0.92	1.68

Xian-Hua et al. [22] published an article in which they examined the properties of gas and char from microwave pyrolysis of pine sawdust. The experiments were conducted using 4 grams of pine saw dust placed into a quartz glass reactor inside a laboratory microwave reactor. The reactor was temperature controlled and experiments took place in a range from 400-800 °C. Elemental analysis of each sample was conducted using a CHNS/O analyzer, while BET surface area analysis was done using an accelerated surface area and porosimetry analyzer. The results shown in Table 2.3.1.7 indicate that as pyrolysis temperature increases carbon content increases while weight percentages of the other main elements reduce or stay low. The results also show BET surface area reducing which is contrary to other studies on the effects of microwave pyrolysis heating temperatures.

Table 2.3.1.7: Elemental and porosity properties of pine sawdust biochar [22]

Temperature / °C	400	500	600	700	800
Volatile	36.45	19.74	16.10	11.23	8.72
Fixed Carbon	63.55	80.26	83.90	88.77	91.28
C	89.35	91.59	92.40	92.85	93.12
H	2.46	2.20	1.39	1.12	0.98
N	0.14	0.20	0.17	0.24	0.23
S	0.34	0.29	0.31	0.27	0.20
O *	7.71	5.72	5.74	5.53	5.47
BET specific surface area / $m^2 \cdot g^{-1}$	0.347	0.276	0.238	0.13	-

Huang et al. [23] studied the process of microwave pyrolysis on rice straw. The study used 3-5 grams of rice straw in a quartz tube microwave reactor at power levels of 50-500 W to determine microwave power level effects. Of the experiments conducted three (300, 400, 500 W) were used to determine the effect of power level on specific surface area and porosity of the biochar. At 300 watts, the heating rate was 55 °C/min while the BET surface area was 165.74 m^2/g. The 400 watt test showed a heating rate of 102 °C/min with SSA of 240.30 m^2/g. Finally the 500 watt test had a heating rate of 141 °C/min and SSA of 274.49 m^2/g. Changes in total pore volume and average pore diameter were negligible throughout the power level. Overall these results indicate a higher heating rate causes a more rapid release of volatiles which produces higher surface area biochar.

The five articles summarized in this section vary in their results but generally indicate that higher biomass heating temperatures/heating rates during microwave pyrolysis will produce biochar with higher BET surface area and pore volume. This data will be taken into consideration throughout this study as producing highly porous biochar is one of the main research goals.

2.3.2 Modulus and Hardness

Das et al. [24] conducted a study on the structure-mechanics of waste derived biochars. The focus of this study was to determine the hardness and elastic modulus of seven different biochars through nanoindentation. The first two samples (TCP900, TCP350) came from pine saw dust that underwent conventional pyrolysis at 900 °C and 350 °C respectively in a two-step auger for 60 minutes. The next two samples (PSD 470, PSD 420)

were also derived from pine saw dust but underwent conventional pyrolysis in a one-step auger for 10 minutes at 470 °C and 420 °C respectively. The fifth sample (biosolids) was processed in a batch reactor at 680°C for 10 minutes. The sixth biochar (Poultry Litter) completed pyrolysis in a continuous auger at 450 °C for 20 minutes. The final sample (BC_Act) was processed in a horizontal batch reactor at 500 °C for 60 minutes.

All seven samples were cold-mounted in epoxy set resin and cured for a day. Each sample was then ground and then polished using higher grits of silicon carbide paper then finally diamond suspended polishing paper. Finally nanoindentation was performed on a Hysitron TI-950 Triboindenter by displacement controlled method with loading and unloading at the same rate of 2000nm/5s. Hardness and modulus was calculated from the load displacement data with material Poisson's ratio assumed to be 0.3. The results of the calculations are shown in Figure 2.3.2.1. From the data it is apparent that high pyrolysis temperature and long heating time plays a direct role in high hardness and modulus values of biochar.

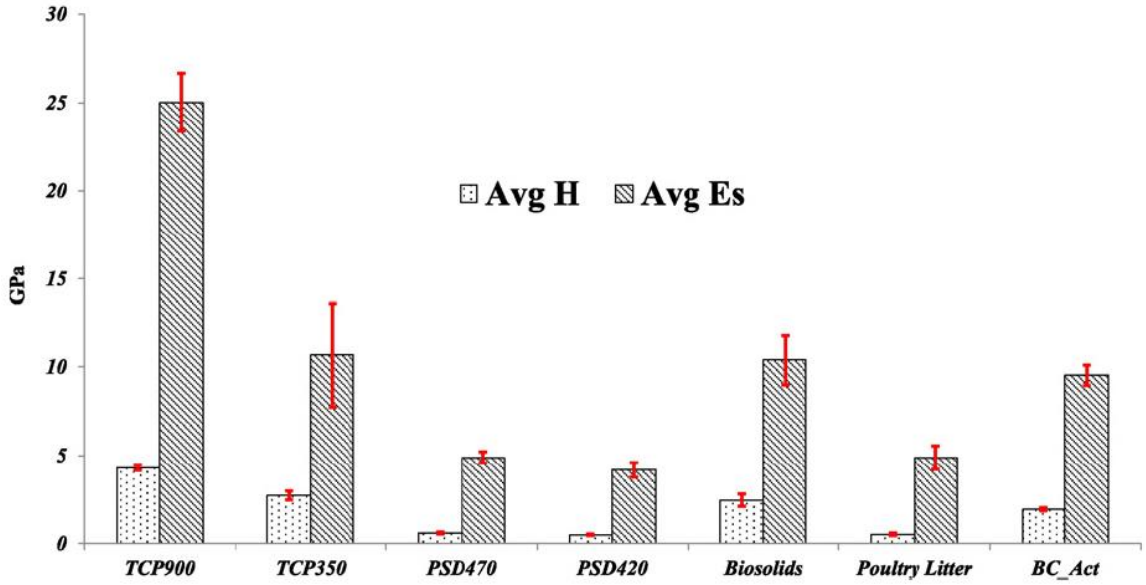

Figure 2.3.2.1: Modulus and hardness data of varying biochar samples [24]

Das et al. [25] published further research detailing the nanoindentation assisted analysis of biochar added biocomposites. In this study pine wood was used as feedstock in an auger reactor at 450 °C and 10 minutes to create biochar. The biochar was used in varying weight percentages (6-30%) as a filler in wood/polypropylene biocomposites. The goal of the study was to take nanoindentation data of each constitute of the three-part biocomposites in order to create models accurately predicting bulk hardness and moduli. From the numerous individual nanoindentation testing of the biochar sample, the average hardness value was 0.43 GPa and the average moduli value was 4.9 GPa. The nanoindentation calculations were conducted while assuming the biochar Poisson's ratio to be 0.3.

Only two articles were identified for this section as the idea of using nanoindentation to determine the hardness and moduli values of biochar is a relatively new topic. Although neither article uses microwave-pyrolysis biochar, they each have data corresponding to

softwood biochar. This data will prove useful as an ideal range for modulus and hardness of softwood derived biochar for this study.

2.4 Composite Testing and Modeling

2.4.1 Biocomposites Strength Testing

The use of biochar as a particulate filler in biocomposites materials is a relatively new concept. In order to prove worthwhile, the new materials will need to have material strength properties exceeding those of the typical composite materials. The following studies all detail the use and mechanical testing of biocomposites materials consisting partially of biochar.

Ogunsona et al. [26] studied the use of biochar from pyrolyzed miscanthus fibers as a reinforcing filler in biocomposites with a bio-based polyamide matrix. The char was produced in a slow pyrolysis process at 500°C. The biocomposites was made through mixing a 20 wt. % of biochar with polyamide and injection molding. Five different biochar particles sizes were used to make the biocomposites. The first two (BC-1, BC-2) were un-sieved and either crushed (<1 mm) or milled (<500μm). The other three (BC-3, BC-4, BC-5) were all milled and sieved (426-500, 213-250, <63μm). The goal of this was to determine the effect of particle size on tensile and flexural strength of the biocomposites. Biocomposites were tested using on a universal testing machine (Instron machine) to determine the mechanical properties. First the specimens were mounted and tested for tensile strength at a crosshead speed of 100 mm/min. Further testing was done to determine the material flexural strength at a crosshead speed of 9.6 mm/min. Figures 2.4.1.1 and

2.4.1.2 detail the resulting strength and modulus characteristics found from testing of each sample. To gain insight to the overall effects of biochar addition, neat polyamide injection molded samples were also tested (PA).

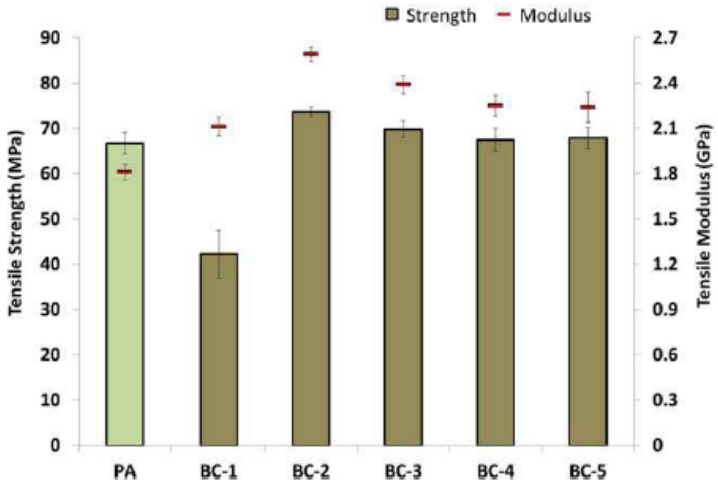

Figure 2.4.1.1: Tensile properties of multiple biocomposites [26]

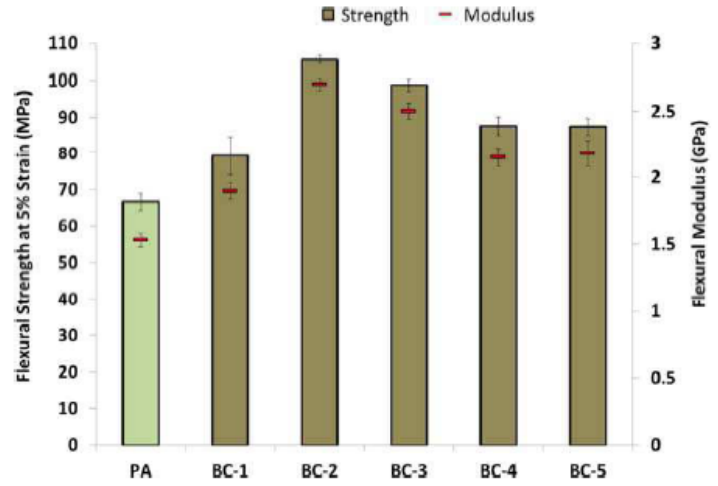

Figure 2.4.1.2: Flexural properties of multiple biocomposites [26]

Analyzing both figures it is noticeable that overall biochar greatly increased both flexural strength and moduli properties of the composite materials. The tensile strength was slightly increased by the addition of biochar in most molds, aside from the case of crushed biochar particles in which it is thought that the large particles size and amount of micropores caused a greater likelihood of cracking, thus lowering the tensile strength. The large increase in flexural strength properties of the biocomposites has been determined to be due to the addition of the harder particles in the soft matrix giving a larger resistance to collapse in the compression region while flexing. This larger resistance to failure is directly related to the higher moduli of the char and increase in surface area contact between the biochar and matrix [26].

Das et al. [4] researched the experimental mechanical testing of biocomposites manufactured with biochar and polypropylene. In this test the biochar was produced from waste pine wood at 500°C. The average carbon content was found to be 82 wt. %, and the specific surface area was 335m^2/g. The biochar was compounded and combined with the polypropylene by injection molding to create said biocomposites. The biocomposites were mostly polypropylene with a range in biochar weight percentage of 15-35%, also one fully polypropylene sample was made for comparison. For testing, the tensile strengths and moduli (chord moduli between 0.05% and 0.25% strain) of each sample were measured on an Intron universal testing machine, and flexural strength and moduli were found using a three-point bending rig in Instron 5567 UTM based on ASTM D790 protocol.

The resulting data shows that both tensile and flexural moduli greatly increase with the addition of biochar. For neat polypropylene tensile and flexural moduli are both approximately 1.5 GPa, while adding 15 wt. % biochar increases them to 2.34 and 2.2 GPa respectively. The largest biochar weight percentage biocomposites (35%) has average tensile and flexural moduli of 3.82 and 3.25 GPa, respectively. These results prove that increasing the amount of harder biochar filler into the soft polypropylene matrix will indeed raise the modulus of the biocomposites. The tensile strength of the biocomposites did not significantly change from the addition of biochar due to a lack of strong interfacial bonding between the particles and matrix, causing the composite to retain the tensile properties of the matrix. Finally, the flexural strength increased due to the addition of biochar, rising from 51.08 MPa when neat polypropylene to 58.26 MPa with 35 wt. % biochar. The increase in flexural strength is determined to be due to the addition of biochar causing a reinforcing effect due to the particle hardness and mechanical interlocking with the polypropylene matrix.

Bowlby et al. [27] performed research on the mechanical testing of pultruded three-part biocomposites consisting of biochar, glass-fiber, and vinyl ester resin. Three separate feedstocks were used in microwave pyrolysis procedures to create the biochar. The feedstocks used were spruce (softwood), maple (hardwood), and Switchgrass (agricultural). The microwave pyrolysis procedure was kept the same for each feedstock. By use of 100 grams of feedstock and 10 grams of biochar as a microwave absorber at 500 watts, an average residence temperature of 700°C was achieved. The resulting chars were tested for specific surface area with spruce being the highest followed by maple then

switchgrass, at 203.9, 155.7, 116.5 m^2/g respectively. Following biochar production and testing, the biocomposites rods were manufactured by mixing the weight percentages (5, 10%) of biochar with the batch of resin, then letting the fibers soak through the resin before being pulled through the heated die of the pultrusion machine. The rods were manufactured from each biochar feedstock species at 5 wt. % and again each at 10 wt. %. For comparison purpose, another six composite rods were created from just the glass fibers and resin.

Flexural testing was done on Instron Model 1332 load frame driven by an Instron 8500 series controller corresponding with ASTM D790 procedure. The resulting strength data is shown in Table 2.4.1.1. The data shows that the addition of 5% biochar vastly increased the flexural strength properties of the biocomposites rods compared to the composite control rods, while increasing to 10% biochar practically doubled the flexural strength. Of note is the correspondence between specific surface area (SSA) of the biochar types and the flexural strength of each. Spruce had the largest measured SSA, and also the largest increase in flexural strength, while switchgrass had the smallest increase in flexural strength and also smallest SSA. This data aligns with the previous literature studies stating an increase of surface area contact between the biochar particles and matrix causes an increase in flexural strength due to potential mechanical interlocking between the two components.

Table 2.4.1.1: Flexural Strength of biocomposites at varying biochar loadings [27]

Biochar reinforcement	Flexural strength (MPa) 5% vol.	Flexural strength (MPa) 10% vol.
Control	450 ± 12	450 ± 12
Spruce	880 ± 17	970 ± 17
Maple	830 ± 16	900 ± 16
Switchgrass	760 ± 14	860 ± 14

This section contained three separate studies on the use of biochar as a particle filler in biocomposites materials. Although the studies were written on biocomposites consisting of different constitutions, the mechanical testing data all agreed that the inclusion of biochar can increase both the moduli and flexural strength parameters of the material. The impact of biochar on composite mechanical properties was determined to be dependent on material hardness and specific surface area of the biochar. The introduction of the hard biochar particles to the softer matrix can increase the material compression resistance during flexural testing as well as provide a mechanical interlocking of the matrix and filler due to high surface area adhesions. These parameters will need to be taken into account while creating the biochar and biocomposites of this study.

2.4.2 Micromechanical Modeling

In order to understand the mechanical properties of composite materials, mathematical models are necessary to predict how a composite will behave under various mechanical loadings. Micromechanical models are powerful tools to understand these properties as a structure will act differently based on its geometry and across the thickness. When discretizing the final structure into unit cells one can pinpoint the local properties, and then using homogenization, connect with the macro-scale global behavior of the composite

structure. The following papers relate to the use of asymptotic homogenization in solving the effective coefficients of fiber-matrix and three-part composite materials.

Kalamkarov et al. [28] proposed and solved an asymptotic homogenization model for three-dimensional composite structures containing a periodic grid of generally orthotropic reinforcements. This micromechanical model is used to solve for the general elastic properties of the composite structure. The basis of the solution make use of the model shown in the left of Figure 2.4.2.1 in which a general composite structure representing an inhomogeneous solid occupying domain Ω with boundary ∂Ω that contains a large number of periodically arranged reinforcements. It is noted that this model is derived from repetition of small unit cell Y in the domain of Ω. The unit cell comprised of a matrix and reinforcing fiber is shown in the right of Figure 2.4.2.1.

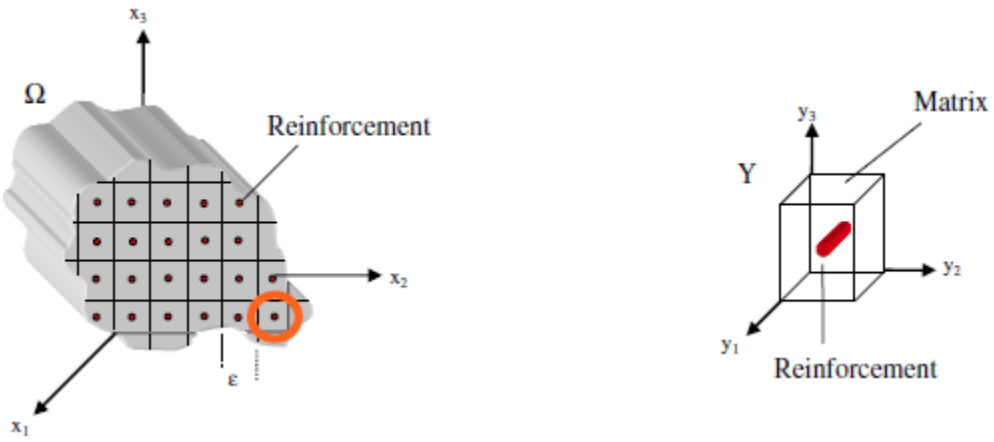

Figure 2.4.2.1: Inhomogeneous solid composite (left) and unit cell matrix model (right) [28]

The elastic deformation of the structure were described by the following boundary value equations.

$$\frac{\partial \sigma_{ij}^{\varepsilon}}{\partial x_j} = f_i \quad \text{in} \quad \Omega, \quad u_i^{\varepsilon}(x) = 0 \quad \text{on} \quad \partial\Omega \tag{2.3.2.1}$$

$$\sigma_{ij}^{\varepsilon}\left(x, \frac{x}{\varepsilon}\right) = C_{ijkl}\left(\frac{x}{\varepsilon}\right) e_{kl}^{\varepsilon}\left(x, \frac{x}{\varepsilon}\right) \tag{2.3.2.2}$$

$$e_{ij}^{\varepsilon}\left(x, \frac{x}{\varepsilon}\right) = \frac{1}{2}\left[\frac{\partial u_i}{\partial x_j}\left(x, \frac{x}{\varepsilon}\right) + \frac{\partial u_j}{\partial x_i}\left(x, \frac{x}{\varepsilon}\right)\right] \tag{2.3.2.3}$$

The summation convention is used throughout this paper with all indexes assuming values of 1, 2, and 3. The value C_{ijkl} is the tensor of elastic coefficients, e_{kl} is the strain tensor as a function of the displacement field u_i, and f_i represents the body forces. The final parameter ε is a non-dimensional unit made by dividing the characteristic size of the unit cell by a characteristic dimension of the overall structure. When analyzing the composite structure on the macroscopic scale, the material constituents are rapidly varying, due to this occurrence a microscale variable was introduced. The inclusion of the fast variable y caused a transformation of the derivatives.

$$y_i = \frac{x_i}{\varepsilon}, \quad i = 1, 2, 3 \tag{2.3.2.4a}$$

$$\frac{\partial}{\partial x_i} \rightarrow \frac{\partial}{\partial x_i} + \frac{1}{\varepsilon}\frac{\partial}{\partial y_i} \tag{2.3.2.4b}$$

The boundary-value problem and corresponding stress field were then transformed to accept both the slow and fast scale variables. All functions in y are collectively periodic with the unit cell Y.

$$\frac{\partial \sigma_{ij}^{\varepsilon}}{\partial x_j} + \frac{1}{\varepsilon}\frac{\partial \sigma_{ij}^{\varepsilon}}{\partial y_j} = f_i \quad \text{in} \quad \Omega, \quad u_i^{\varepsilon} = 0 \quad \text{on} \quad \partial\Omega \tag{2.3.2.5}$$

$$\sigma_{ij}^{\varepsilon}(x, y) = C_{ijkl}(y)\frac{\partial u_k}{\partial x_l}(x, y) \tag{2.3.2.6}$$

Second order asymptotic expansions were then setup in terms of the small parameter ε for the displacement field and stress field. Solving these from the use of the boundary-value and stress field equations, a series of differential equations was found.

$$\frac{\partial \sigma_{ij}^{0}}{\partial y_j} = 0 \tag{2.3.2.7a}$$

$$\frac{\partial \sigma_{ij}^{1}}{\partial y_j} + \frac{\partial \sigma_{ij}^{0}}{\partial x_j} = f_i \tag{2.3.2.7b}$$

Where

$$\partial\sigma_{ij}^{0} = C_{ijkl}\left(\frac{\partial u_k^0}{\partial x_l} + \frac{\partial u_k^1}{\partial y_l}\right) \tag{2.3.2.8a}$$

$$\partial\sigma_{ij}^{1} = C_{ijkl}\left(\frac{\partial u_k^1}{\partial x_l} + \frac{\partial u_k^2}{\partial y_l}\right) \tag{2.3.2.8b}$$

Upon combining equations (7a) and (8a) and then separating variables, the following equation was found for the solution of the displacement field u^1.

$$u_m^1(x,y) = \frac{\partial u_k^0(x)}{\partial x_l} N_m^{kl}(y) \tag{2.3.2.9}$$

Where functions N_m^{kl} are periodic in y and satisfy

$$\frac{\partial}{\partial y_j}\left(C_{ijmn}(y)\frac{\partial N_m^{kl}(y)}{\partial y_n}\right) = -\frac{\partial C_{ijkl}}{\partial y_j} \tag{2.3.2.10}$$

Equation (2.3.2.10) is referred to as the unit cell problem as it depends entirely on the fast variable y and is solved on the domain Y of the unit cell. Both C_{ijkl} and N_m^{kl} are Y-periodic in y. The homogenization procedure was then carried out by substituting (2.3.2.10) into (2.3.2.8a) then integrating over the domain Y of the unit cell (with volume |Y|) treating x_i as a parameter for integration with respect to y_j. Homogenization yielded

$$\frac{1}{|Y|}\int_Y \frac{\partial \sigma_{ij}^1(x,y)}{\partial y_j} dv + \tilde{C}_{ijkl}\frac{\partial^2 u_k^0(x)}{\partial x_j \partial x_l} = f_i \tag{2.3.2.11}$$

Where the following definition was introduced

$$\tilde{C}_{ijkl} = \frac{1}{|Y|}\int_Y \left(C_{ijkl}(y) + C_{ijmn}(y)\frac{\partial N_m^{kl}}{\partial y_n}\right) dv \tag{2.3.2.12}$$

The coefficients $\tilde{C}_{ijkl}$ denote the homogenized or effective elastic coefficient. These effective coefficients are universal in nature and can be used to study a wide variety of boundary value problems associated with a given composite structure. The paper goes on to numerically solve some examples of effective elastic coefficients of grid reinforced structures based upon volume fraction of the reinforcements [28].

De et al. [29] analyzed the use of asymptotic homogenization techniques to predict the elastic properties of unidirectional fiber-reinforced composites. Starting with the same homogenized effective coefficients derived by Kalamkarov et al. [28], the authors solve for auxiliary displacement fields from which they then solve for stiffness and load vectors. The composite material analyzed for this study was comprised of E-Glass 21xK43 Gevetex (glass fiber) and LY556/HT907/DY063 (epoxy matrix). Elastic properties of the individual constituents were known from the supplier. Using finite element method software and known stiffness values of the materials, elastic properties calculated through asymptotic homogenization were found based upon the hexagonal FEM mesh and representative volume element (RVE) in Figure 2.4.2.2.

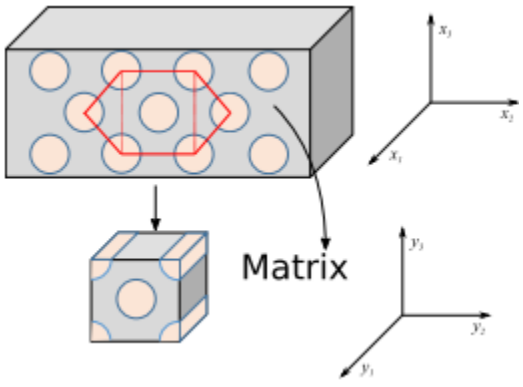

Figure 2.3.2.2: Composite mesh and RVE [29]

The resulting elastic properties was compared with experimental data published by Soden et al. [30] detailing their work with composite materials comprised of the same constituent materials. The resulting data was a comparison of the elastic properties derived from the asymptotic model and from experimental results for varying fiber volume fractions. For the following results E, G, and v are respectively the elastic modulus, shear modulus, and Poisson ratio. The comparison for calculated and experiments results was closest at a 69% fiber volume fraction with 4.8, 9.8, 1.5, 8.3, and 14.4 % difference for E_1, E_2, G_{12} (GPa), v_{23}, and v_{12} respectively. The average percent difference between the calculated and experimental elastic properties for this composite was 7.7%. This data gives proof that the asymptotic homogenization method can be used in micromechanical modeling to accurately predict fiber-reinforced composite elastic properties.

The two scholarly articles summarized in this section give some insight into the use of homogenization as a micromechanical modeling tool for fiber-reinforced composite materials. Further articles go on develop these models to predict mechanical properties of other two and three-phase composite shapes and structures.

Chapter 3

Methodology

This section is dedicated to providing a detailed explanation of the requirements and processes carried out to complete the research methodology of this study. Figure 3.1 below shows a high level process flow of the methodology steps. Each step will be further expanded on throughout the section.

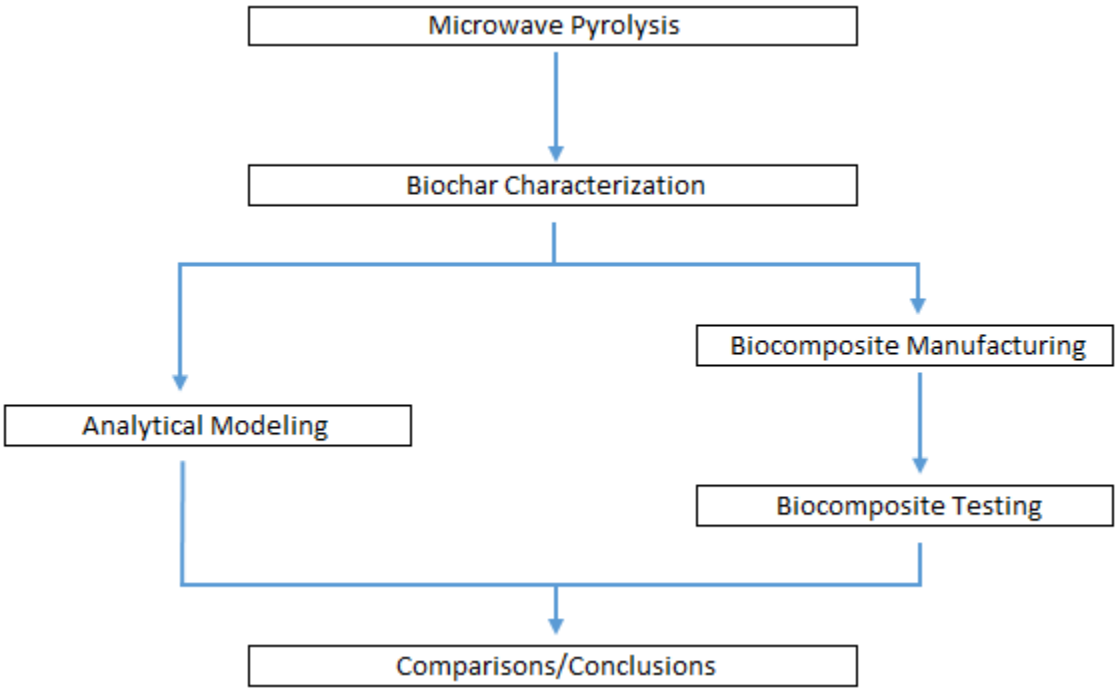

Figure 3.1: Research process flow

3.1 Microwave Pyrolysis

3.1.1 Materials

Two biomass feedstocks were chosen for use in this study. The first feedstock is a combination of spruce and fir softwood chips donated by Devon Lumber Company. New Brunswick has a large softwood industry, and the use of waste softwood chips for this study could provide the industry with another option for the recycle and use of waste chips. Additionally, the use of softwood biomass for microwave pyrolysis is well documented with the resulting biochar showing quality surface area and porosity characteristics [22, 27]. Shown on the left side of Figure 3.1.1.1 the chips were in a variety of non-uniform sizes. Moisture content was tested using ASTM E1756 standard procedure. The samples used for this study were found to be at a moisture content of approximately 12%.

Figure 3.1.1.1: Biomass feedstocks

The second feedstock used in this study is hemp straw. Hemp is a promising energy crop due to its rapid growth rate and high biomass yield [31]. The donated hemp arrived in a large bail which was stored and dried. For each sample, dried hemp was pulled from the

bail and hand shredded to the state shown on the right side of Figure 3.1.1.1. Using the same testing method, moisture content for the hemp was found to be approximately 13%.

3.1.2 Experiment Preparation

The microwave pyrolysis experiments in this study were ran in a large single-batch reactor as shown in Figure 3.1.2.1. Microwaves are generated by a Muegge GmbH microwave generator and sent through a waveguide into the insulated reactor. As the feedstock is heated, vapor and oil exit through the bottom outlet into the condenser. Prior to and throughout the experiments, nitrogen gas was fed through the top in order to expel any oxygen out of the reactor. For each experimental test, 1000 grams of biomass was weighed and used as feedstock. Considering that the dryness of each feedstock gives poor microwave absorption, biochar from previous experiments was added to the reactor as a microwave absorbing catalyst at 10 weight percentage. In order to give a relatively even spread of the microwave absorbers, 500 grams of the feedstock was placed in the cylindrical reactor, followed by 100 grams of the absorber, then the final 500 grams of feedstock.

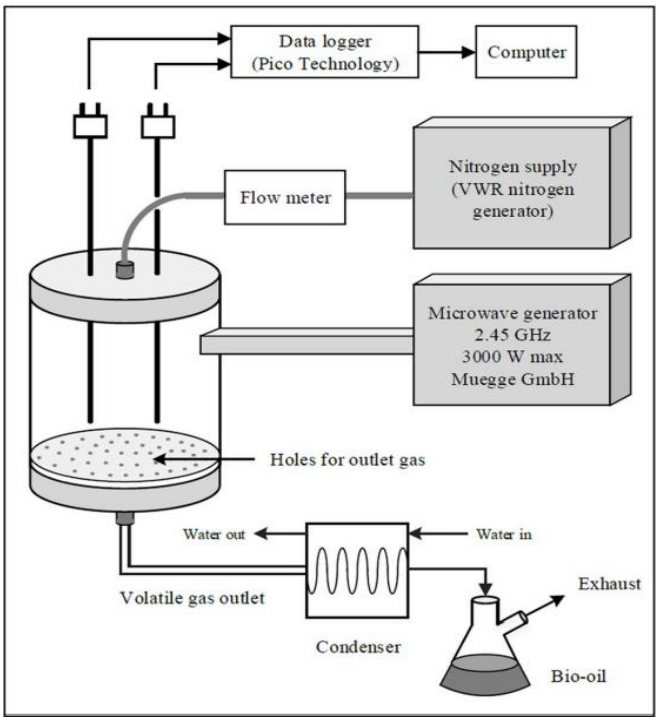

Figure 3.1.2.1: Microwave pyrolysis system used in the study

Following feedstock preparation, the top lid of the reactor was sealed by a combination of aluminum foil tape and clamps. The two thermocouples were then fed through small lid inlets and taped into place with the aluminum foil tape. The hose of the nitrogen generator screwed into a threaded inlet of the lid and the nitrogen generator was started. In order to ensure an anaerobic environment, the nitrogen flowed for approximately 45 minutes prior to testing and continued to flow throughout. Once the nitrogen had been flowing long enough, condenser water and microwave cooling water were both ran. The condenser water flowed from a tap and was generally 14˚C. The microwave cooling water was kept at 20˚C and a flow rate of 4.5L/min.

3.1.3 Design of Experiments

Based on multiple preliminary experiments, three power levels of 2100, 2400, and 2700 watts were chosen for experimentation in this study. These power levels were deemed suitable because they give a good spread of 300 watts each and also represent 70, 80, and 90% of the microwave generators maximum 3000 watt power level. This separation of chosen power levels also provided insight into microwave pyrolysis power efficiencies of the experiments.

Due to the difficulties in measuring temperature data during microwave experiments, the designated power levels were each tested a minimum of three times in order to achieve acceptable temperature data for a minimum total of 18 tests. The microwave generator was ran for one hour each test, and only microwave power level varied as all other parameters were kept the same. The design of experiments for microwave pyrolysis is displayed below in Table 3.1.3.1

Table 3.1.3.1: Microwave pyrolysis design of experiments

Experiments	Feedstock	Power Level (Watts)
1	Softwood	2100
4 - 6	Softwood	2400
7 - 9	Softwood	2700
10 - 12	Hemp	2100
13 - 15	Hemp	2400
16 - 18	Hemp	2700

During experiments temperature data was actively recorded and monitored using the Pico Technology data logger and thermocouple. The recorded temperature profiles varied from

experiment to experiment due to the difficulties of using a metal thermocouple in a microwave reactor. The position of the thermocouple was highly important as it must be placed in densely packed feedstock in order to accurately measure the reaction temperature. The temperatures may also spike or settle based on areas of random microwave hot spot inside the reactor, as well as the possibility of hot spots occurring from reactions between the metal thermocouple and electromagnetic waves [6]. These temperature measurement issues are common to microwave pyrolysis studies [6, 27], and every effort was made to ensure the accuracy of recorded data.

3.1.4 Post-Experiment

After stopping the microwave generator and closing the recording software, the resulting biochar was allowed to cool inside the reactor for at least 4 hours. During this time the nitrogen is still running and the reactor is kept sealed to ensure the environment is anaerobic. Once the condenser bulb is cool enough, it is removed and the collected bio-oil was measured then stored. The emphasis of this study was not on bio-oil but the collected weight data is useful for yield studies and to estimate the efficiency of the condenser. Once the biochar has cooled inside the reactor for long enough, it was also removed and weighed. Again this weight data was used to determine the yield percentage of biochar at each power level. The biochar was then packaged in reusable containers and stored for future characterization.

3.2 Biochar Characterization

The biochar samples produced in this study underwent a number of common characterization tests in order to compare the qualities of the produced char with that of

previous studies, as well as gain insight on how the varying microwave system power levels affect certain key biochar properties. The results of the characterization tests were also used in comparison with biocomposites testing data to develop an assessment of biochar factors affecting its use as a particulate filler.

3.2.1 Porous Properties

Surface properties of the biochar were analyzed using the Brunauer, Emmett, and Teller (BET) surface area analysis method in which nitrogen gas is used as an absorbent in a physiosorption procedure. The resulting data from this test includes specific surface area (m^2/g), porosity distribution (cc/g), and average pore size (Å). Further insight to the quality of the biochar surface structure was found through scanning electron microscopy (SEM) in which high resolution images of the char is taken at large magnifications. Analysis of these images for cracks on the honeycomb structure or adhesions from unwanted volatiles in the pores helped determine the quality of produced biochar.

3.2.2 Elemental and Ash Analysis

Elemental analysis of biochar was performed using a CHN Elemental Analyzer according to ASTM D5373 standard procedure. High weight percentage of carbon content is an indicator of higher strength quality biochar and therefore the main interest of this characterization test. Ash content of biochar is also an important characteristic as a high ash content is associated with a more brittle biochar which is prone to cracks and fissures. Ash content (dry basis), along with other proximate analysis characteristics, was measured in a muffle furnace using ASTM D1762-84 standard procedure. Fourier transform infrared spectroscopy was also performed

to determine the composition of the chars and feedstocks, and evaluate the loss of major functional groups in the feedstock after pyrolysis.

3.2.3 Hardness and Modulus

The hardness of a material is a measure of the materials resistance to deformation by indentation, while the elastic modulus is a measure of the materials resistance to elastic deformation. Both of these properties were measured for biochar by cold-mounting the char is an epoxy resin, grinding and polishing the sample with decreasing grit sizes from 500 to 1200 microns, and testing the sample through a nanoindentation technique. Results from this characterization test provided key correlations between the pyrolysis heating levels and mechanical properties of the biochar, and also between the mechanical properties of the biochar and mechanical properties of the biocomposites.

3.3 Biocomposites Manufacturing and Testing

3.3.1 Pultrusion Machine and Materials

The biocomposites rebar rods for this study were manufactured with a pultrusion machine, specifically the modified in house pultruder shown in Figure 3.3.1.1. Roving from 22 spools of E-Glass fiber were pulled through the vinyl ester resin bath, then through the heated die by the end pulleys as shown. The finished rods exited the pulley with an approximate diameter of 9.3mm and were cut to preferred lengths. The steel die is heated by 12 electric strip heaters, in pairs of two along both the top and bottom portions. Each pair of strip heaters is controlled through feedback of a thermocouple with a PID controller. The programmed temperatures and nominal pulling speed of the motor driven pulleys is

shown in Table 3.3.1.1. These optimal parameters were found through previous research utilizing the machine [27].

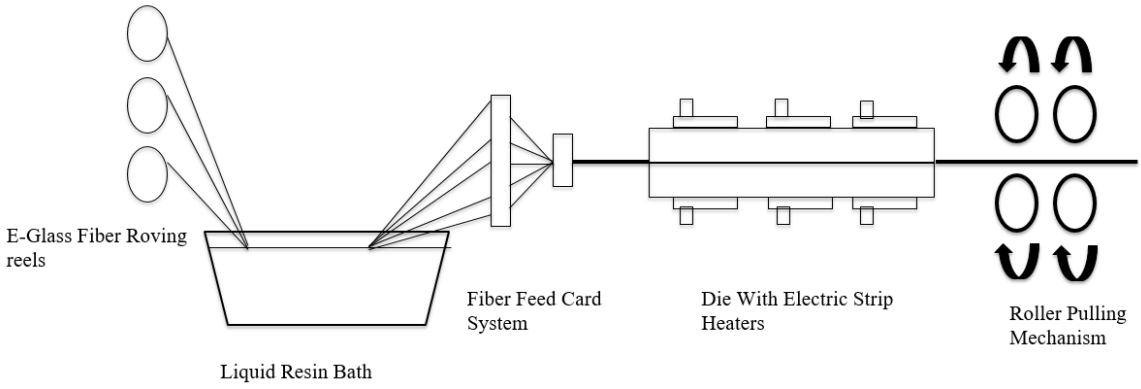

Figure 3.3.1.1: Pultrusion machine, Nanocomposites and Mechanics Lab

Table 3.3.1.1: Pultrusion operational parameters

Parameter	Operating Value
Pull Speed	30 cm/min
Heater Set (1)	120°C
Heater Set (2)	150°C
Heater Set (3)	150°C

The base constituents of the composite rods were E-glass fibers, sourced from Fiber Glass Industries under the trade name Flexstrand 700, and vinyl ester resin sourced from Reichold Chemical under the trade name urethane modified biphenyl vinyl ester. Material mechanical information for the two constituents is found below in Table 3.3.1.2.

Table 3.3.1.2: Composite materials properties

E-Glass Fibers		Vinyl ester Resin	
Tensile Strength (MPa)	2760	Tensile Strength (MPa)	73
Tensile Modulus (GPa)	73	Tensile Modulus (GPa)	3
Poisson's ratio	0.22	Poisson's ratio	0.4
Diameter (microns)	23	Flexural Strength (MPa)	156
Density (g/cm^3)	2.54	Flexural Modulus (GPa)	3.2

Along with the vinyl ester resin, three organic peroxide initiators and a lubricant were mixed into the resin bed. The purpose of the peroxide initiators are to initiate the polymerization reaction of the resin through heat activation in the die. The lubricant was also used in small quantities to ensure easy movement of the fibers through the die. The organic peroxides and lubricant used are summarized in Table 3.3.1.3.

Table 3.3.1.3: Pultrusion initiators and lubricant

Material	Product
Initiator 1	Technick Products 190-TG
Initiator 2	United Initiators NOROX PULCAT AMB
Initiator 3	United Initiators t-BPB
Lubricant	United Initiators 500-750MS

3.3.2 Design of Experiments

As the purpose of this study was to research the mechanical property effects when using biochar as a particulate filler in glass-fiber reinforced polymers, different weight percentage loadings of biochar were needed for comparison. In order to compare the transverse and axial properties of the biocomposites with the plain glass-fiber polymer

control rods, every biocomposites had the same fiber loading as the control rods. Keeping the glass fiber loading the same for every rod caused the matrix loading to decrease as biochar loading increases. In order to control the range of experiments, only biochar from the 2700 watt pyrolysis runs was used for biocomposites manufacturing. A summary of the design of experiments as it pertains to biochar/matrix material percentage loadings is shown in Table 3.3.2.1.

Table 3.3.2.1: Biocomposites manufacturing design of experiments

Specimen	Biochar Feedstock	Vinyl ester Resin Volume Fraction (%)	Biochar Particle Volume Fraction (%)
S.C1	None (control)	100	0
S.S1	Softwood	95	5
S.S2	Softwood	90	10
S.S3	Softwood	80	20
S.H1	Hemp	95	5
S.H2	Hemp	90	10
S.H3	Hemp	80	20

As shown in the design of experiments, three biochar particle loadings were chosen for this study. The first two loadings of 5, and 10%, were picked in for comparison purposes with previous studies [27]. The final loading of 20% was determined in order to gain some insight of maximum loading values. Due to the fact that increase in biochar loading percentages causes a decrease in the amount of vinyl ester matrix, there was some concern of biocomposites rod matrix quality at high biochar levels, therefore the 20% volume fraction not only gave insight to rod quality but also helped determine if there is an optimal

biochar loading for the biocomposites in relation to improved material properties. Furthermore, the biochar used for biocomposites manufacturing will be first grinded, then sieved to ensure that biochar particles less than 425 microns are used for production. The mean particle size of each biochar will also be measured prior to use.

3.3.3 Biocomposites Testing

In order to gain an understanding of the mechanical effects of biochar as a particle filler in GFRP biocomposites, the manufactured rods underwent both flexural and tensile testing using an Instron testing machine. Flexural testing is performed in a three-point-bending jig with test parameters (strain rate, sample length, and span) set to accordance of ASTM D790. Composite stress and strain data was gathered and analyzed, for six tests per sample, to describe a statistical average of the effects from biochar loading on the flexural yield strength and modulus of the biocomposites.

Tensile testing setup was complex owing to the smooth, cylindrical shape, and high tensile strength of the biocomposites. Three test specimen for each biochar type and loading were first selected at 760mm lengths. Anchorage lengths of 270 mm were coated at each end of the biocomposites with epoxy, then sand coated with course sand, previously sieved to pass through a 1.25mm and retained by a 1.18mm sieve. Two lengths of schedule 160, 1-inch steel piping were cut to 270mm for each of the biocomposites. Pin holes of 9/16 inch diameter were drilled through the bottom of each pipe for later testing. Once the sand-coating had cured, the composite were placed one end at a time, into the steel piping, held up by the curing jig in Figure 3.3.3.1. The piping was filled with RockFrac expanding

mortar, which then was allowed to cure a minimum of 48 hours to its maximum expanded pressure specified to be 150 MPa.

Tensile testing was performed by pinning each end of the composite/pipe setup to the base and crosshead of an Instron universal testing machine. Displacement controlled testing was performed at a loading rate of 2mm/min. An integrated load cell measured tension force while a 50 mm gauge length Instron extensometer placed at mid-span of the bars measured strain. Testing was performed two times per biocomposites type, with an additional tensile test performed for each sample, with the same test parameters, using a digital image correlation (DIC) technique measure strain. DIC has been shown to provide accurate measurements of strain on composites in this application [32].

Figure 3.3.3.1: Tensile curing jig

3.4 Biocomposites Modeling

Biocomposites modeling for this study was completed using two separate micromechanical models, the first being the rule of mixtures. For two-part composites a common predictive method is the rule of mixtures (Equation 3.4.1). This theory builds off of the iso-stress model and indicates that the composite modulus (E_c) is a combination of the fiber (E_f,) and matrix constituent's individual moduli (E_m) versus their individual composite volume fractions (V_f, $V_{m)}$ [10].

$$E_c = E_f V_f + E_m V_m \quad (3.4.1)$$

Assumptions made when using the rule of mixtures equations include: uniform dispersion of fibers, perfect bonding between fibers and matrix, and matrix is free of voids [10]. In order to utilize the rule of mixtures model for the current three-part biocomposites, further assumptions were made that the mixture of biochar powder into the vinyl ester resin prior to pultrusion created a new complex matrix for which rule of mixtures could also be used to calculate the new matrix modulus as in Equation 3.4.2, where subscripts bc, and r indicate the biochar and resin contributions. Using the new matrix modulus, the total biocomposites modulus was calculated from rule of mixtures as in Equation 3.4.1.

$$E_m = E_{bc} V_{bc} + E_r V_r \quad (3.4.2)$$

A more advanced predictive method used for finding the effective elastic moduli of the biocomposites was also employed through homogenization of a representative volume element (RVE). RVE models for both the biochar/resin matrix, and the total biocomposites were compiled and analyzed through Abaqus FEA software [33], by applying a uniform strain to each RVE and solving to find the individual nodal stresses and strains of the RVE mesh. Homogenization calculations [34] were completed, according to Equations 3.4.3 and 3.4.4, to find the effective stress (σ_{11}) and strains (ε_{11}) in the fiber direction of the models, where v^k is the integration point volume of the mesh, and V is the total volume of each RVE.

$$\sigma_{ij} = \frac{1}{V}\int_V^1 \sigma_{ij}\, dV = \frac{1}{V}\sum_{k=1}^{N_p} \sigma_{ij}^k v^k \quad (3.4.3)$$

$$\varepsilon_{ij} = \frac{1}{V}\int_V^1 \varepsilon_{ij}\, dV = \frac{1}{V}\sum_{k=1}^{N_p} \epsilon_{ij}^k v^k \quad (3.4.4)$$

The effective elastic modulus of the composite was then found by dividing the homogenized stress by the homogenized strain. In order to use these micromechanical models, the individual modulus of the E-glass fibers and vinyl ester resin (Table 3.3.1.2) was used in conjunction with the experimental modulus of biochar samples found through nanoindentation method.

Biocomposites modeling consisted of two components the first being the biochar-matrix RVE model, and the second being the single fiber biocomposites RVE model. Some assumptions were made in-order to simplify the FEA models, including: periodic and regularly spaced fibers and biochar particles, all constituents are elastic in nature, fibers and particles are homogeneous and perfectly bonded to the matrix, biochar particles are spherical and solid, the composite is free of voids or irregularities [35]. Assuming a homogenous and periodic biochar mixture inside the resin, a square RVE model was chosen for the biochar/resin matrix model as shown in Figure 3.4.1. Abaqus models were then made by using a 100 unit^3 cubed matrix model, and adjusting the spherical biochar particle dimensions to represent 5, 10, and 20% char volume inside the matrix. Figure 3.4.2 displays the Abaqus RVE model used to represent 10% biochar matrix.

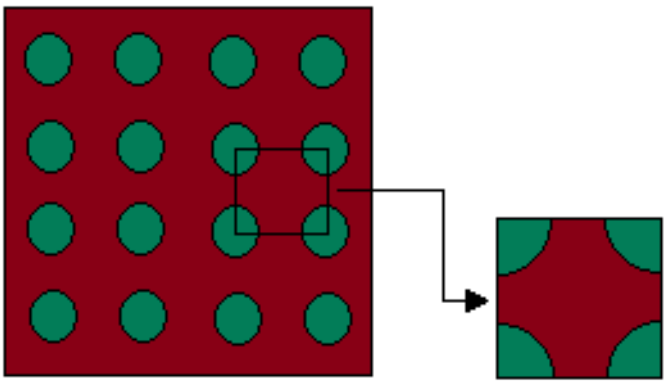

Figure 3.4.1: Particle - matrix RVE model

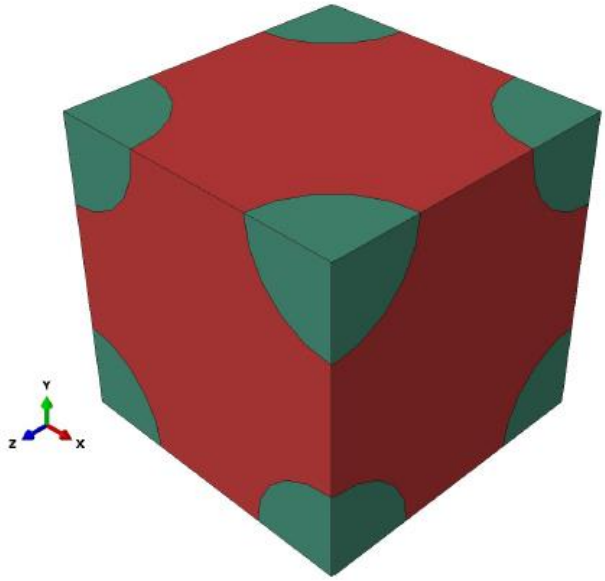

Figure 3.4.2: Abaqus particle-matrix RVE model

For homogenization of unidirectional fiber reinforced composites, single fiber unit-cell models are often chosen due to the simplicity of the RVE model allowed by the assumption of periodically spaced fibers [34]. Figure 3.4.3 displays the unit-cell RVE model, containing a single cylindrical fiber surround by matrix material. The fiber-matrix model

was created in Abaqus, as a cubic RVE of dimensions 50x50x10 units^3, and the fiber diameter calculated to represent 62% of the composite volume fraction. The length of the fiber was chosen as 10 units in order to reduce computational time by reducing the total mesh size [35]. In order to develop the RVE into the biocomposites model, the biochar/resin model was positioned periodically to create the cubic shape into which the fiber is centered (Figure 3.4.4).

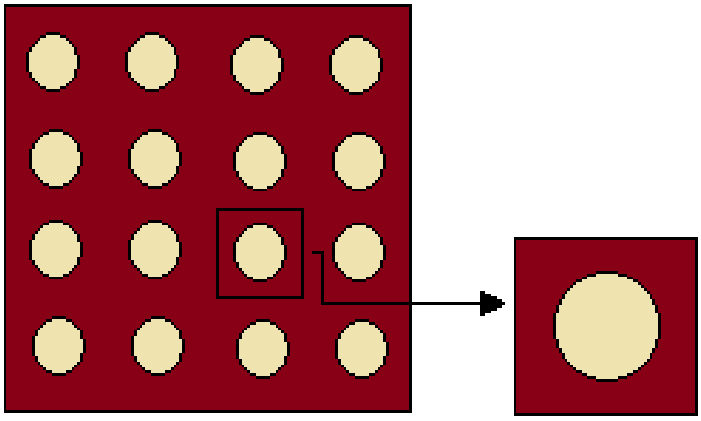

Figure 3.4.3: Single fiber RVE model

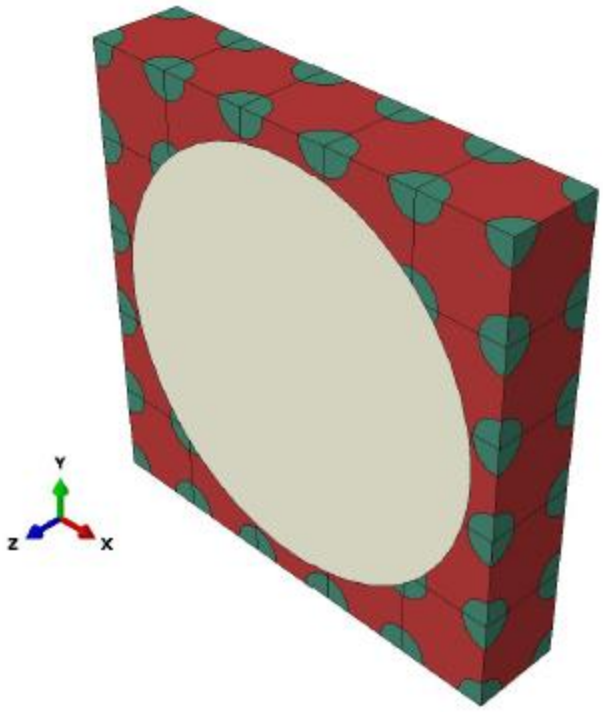

Figure 3.4.4: Abaqus composite RVE model

The biocomposites models were created representing 5, 10, and 20% biochar matrix volume percentage, and material properties (young's modulus, poisons ratio) were assigned to all the components based on their individual constitute properties. Owing to the spherical shape of the biochar particles, a tetrahedron mesh was assigned to the models. Assuming perfect bonding of all the biocomposites constituents, cohesive bonding constrains were added to the model components. Finally, in-order to facilitate the usage of Hook's Law to solve for the effective modulus in the fiber-direction, a uniform strain was given according to Equation 5, as shown in Figures 3.4.5 and 3.4.6.

$$\begin{pmatrix} x \\ y \\ z \end{pmatrix} = \begin{bmatrix} 0 & 0 & 0 \\ 0 & 0 & 0 \\ 0 & 0 & 1 \end{bmatrix} \begin{pmatrix} x \\ y \\ z \end{pmatrix} = \begin{pmatrix} 0 \\ 0 \\ z \end{pmatrix} \quad (3.3.5)$$

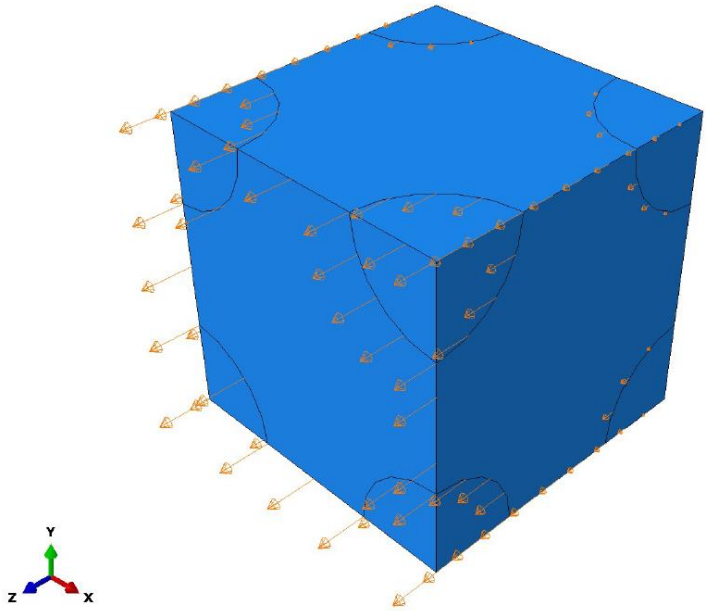

Figure 3.4.5: Abaqus particle-matrix uniform strain

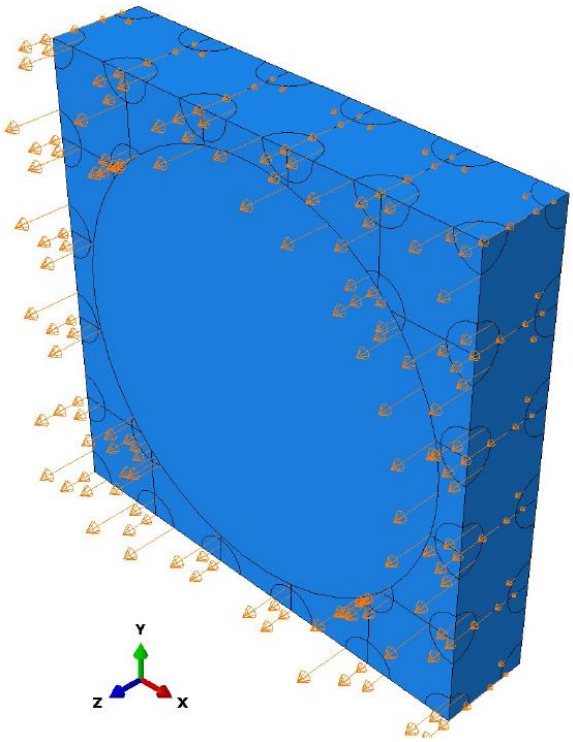

Figure 3.4.6: Abaqus composite uniform strain

Upon solving each model through Abaqus, data files were processed and compiled in Matlab through the usage of the Abaqus2Matlab plug-in [36]. Matlab code was included to first extract the stress (E_{33}), Strain (ε_{33}), and integration point volume (IVOL) data for the solved RVE model, which was then used for homogenization calculations (Equations 3.4.3., 3.4.4) to compute the composite model effective stress, strain, and finally homogenized modulus. The Matlab homogenization code can be found in Appendix D.

Chapter 4

Results & Discussion

The following section describes and discusses all results pertaining to the goals of this study. Figure 4.1 below are samples from the collected biochar. For both softwood and hemp developed char has a shiny black tint and mostly retained its original structure. Prior

Figure 4.1: Softwood (left) and hemp (right) biochar samples

to biocomposites manufacturing, biochar from each was grinded and sieved to a mean particle size of 190 and 230 microns for softwood and hemp respectively. Figure 4.2 displays a single control rod alongside a biocomposites containing 20% biochar loadings. Noticeably biocomposites rods follow the same black tint under their glassy surface finish.

Figure 4.2: Biocomposites and control rod

4.1 Pyrolysis Temperature Profiles and Data

Figures 4.1.1 and 4.1.2 detail the average temperature profiles for the tests varying power level and for each biomass feedstock. The temperature profiles represent an average of three data sets at each power level. The profiles all follow a similar trend of varying heating rates followed by long lengths of residence temperatures when scaled-up, as power increases. The existence of more erratic peaks at higher power levels is a common occurrence and can be attributed to the increasing presence of potential microwave hotspots, as well as the potential for reaction between the metal thermocouple and

electromagnetic field at these elevated power levels [6, 27], as well as the thermocouples maximum temperature rating of 1300 °C. Comparing the hemp temperature profiles to the softwood temperature profiles it is noted that overall the hemp profiles are more uniform throughout each power level, this could be due to a more uniform contact between the thermocouple and biomass for hemp compared to softwood, as the shredded hemp can be more densely packed into the reactor than the non-uniform softwood chips. Individual temperature profiles for each test per power level can be found in Figures B1 through B6 in Appendix B.

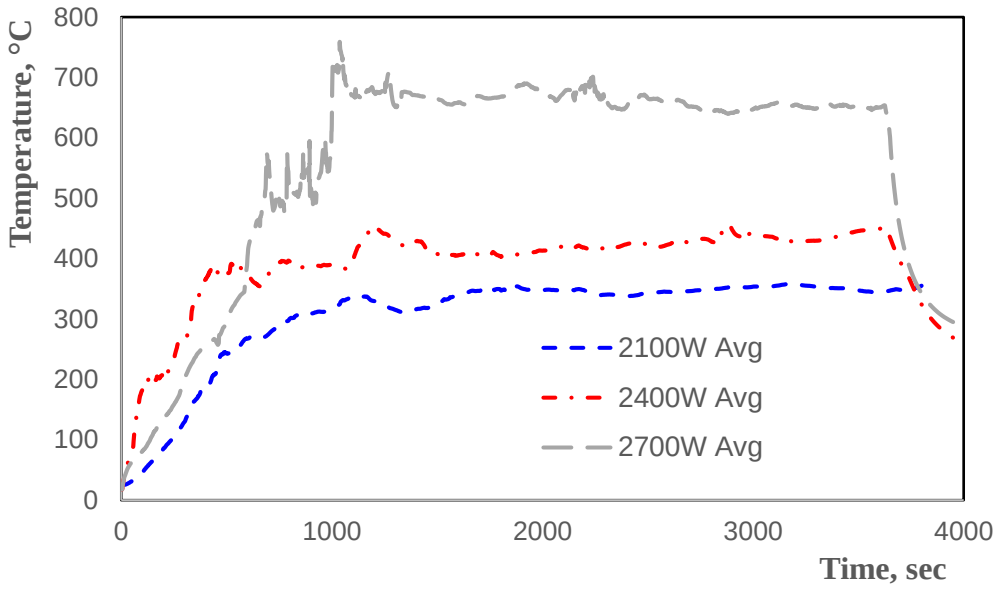

Figure 4.1.1: Softwood pyrolysis temperature profiles

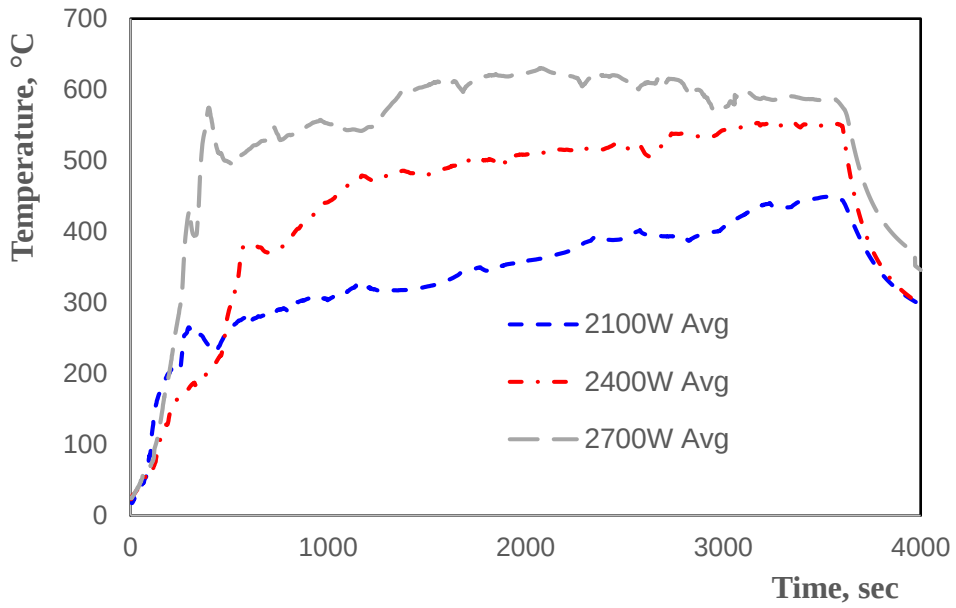

Figure 4.1.2: Hemp pyrolysis temperature profiles

Table 4.1.1 details the average heating rate and residence temperature of each test. For this study, the heating rate is considered to be rate of rise in temperature during the first ten minutes of the experiment (°C/min) and the residence temperature is considered to be the average temperature during the last thirty minutes of the hour long experiment (°C). For the softwood, there is a notable increase in residence temperature when power level increased from 2100 to 2400 Watts, and even a larger rise from 2400 to 2700 Watts. On the contrary, hemp profiles display a large increase in residence temperatures between 2100 to 2400 Watts, with a smaller but steady increase between 2400 and 2700 Watts. The power levels of 2100, 2400, and 2700 Watts were selected upon completion of several preliminary tests determining the minimum power required to convert the biomass to biochar through pyrolysis. These power levels are correspondingly 70, 80, and 90 percentage of the microwave's maximum power supply limit. The range of heating rates and residence

temperatures of pyrolysis during this study will be important when describing the characteristics of the produced biochars.

Table 4.1.1: Pyrolysis temperature data

Sample designation	Heating rate, ^{o}C/min	Residence temperature, ^{o}C
SW-2100W	24.5 ± 4.9	348.4 ± 33.9
SW-2400W	35.1 ± 3.6	427.5 ± 31.2
SW-2700W	42.8 ± 13.4	659.8 ± 60.0
HM-2100W	25.4 ± 3.9	398.8 ± 38.7
HM-2400W	35.5 ± 12.6	528.7 ± 13.2
HM-2700W	49.1 ± 10.8	604.2 ± 10.8

Studies performing microwave pyrolysis in small-batch quartz crucible reactors, utilizing softwood feedstocks, have shown similar residence temperature at much lower microwave powers of 300 to 700 Watts [13-15]. These same studies, which usually utilized 5-15 grams of raw biomass, reported the large heating rates ranging 120-240 ^{o}C/min. Comparing the literature results with the current results in the large batch, 1000 gram reaction, indicates the need for much higher microwave power levels, as well as longer residence times (due to the slower heating rates) in order to attain similar residence temperatures in a large-batch microwave pyrolysis process.

4.2 Biochar Yield Data

Table 4.2.1 contains the average biochar yield data from each power level per feedstock. This data was recorded from collecting and weighing the solids after each pyrolysis reaction and comparing to the original weight of the solid feedstock in the reactor. As shown for both feedstocks, an increase in power level leads to decreases of char yield percentages. The elevated heating rates and residence temperatures cause a faster and larger release of volatiles in the form of liquids and gas, leaving smaller weight percentages of solids [5]. The data found from these experiments follow trends from similar studies [13, 14].

Table 4.2.1: Biochar yield per microwave power level

Microwave power level, Watts	Softwood biochar, wt.%	Hemp biochar, wt.%
2100	40	37
2400	30	33
2700	24	27

4.3 Biochar Chemical Properties

4.3.1 Ultimate and Proximate Analysis

Table 4.3.1.1 provides the proximate and ultimate analyses of the biochar produced at different power levels. Proximate analysis details the weight percentages of moisture content, volatile matter, fixed carbon, and ash in the char samples. The results indicate a decline in volatile matter and increase in fixed carbon content as power level increases,

relating to higher heating rates and residence times. This reverse trend between volatile matter and fixed carbon is often reported [23], and is due to the decomposition of lignocellulosic functional groups [20] which exit the biomass at higher rates correlated to the heating rate of the pyrolysis process [8]. Comparing the volatile matter in the raw feedstock to their biochar, there is a large decline. This is again due to the major loss of lignocellulosic groups exiting the microwave system as bio-oil and gaseous products while the biomass carbonizes.

Table 4.3.1.1: Comparative analysis of chemical properties in biochar obtained from softwood and hemp

Sample	Proximate analysis, wt.%				Ultimate analysis, wt.%			
	Moisture content	Volatile matter	Fixed carbon	Ash	C	H_2	N_2	O_2
Softwood (raw)	11.5	67.3	19.5	1.7	44.43	6.16	0.18	49.23
Hemp (raw)	10.7	69.6	18.8	0.9	45.71	5.89	-	48.40
SW-2100	4.8	32.1	60.0	3.1	79.97	3.53	0.01	16.49
SW-2400	4.7	29.2	61.3	4.8	79.82	3.55	0.01	16.62
SW-2700	3.9	25.0	69.1	2.0	77.48	3.64	0.10	18.78
HM-2100	2.8	27.6	66.8	2.8	78.19	3.22	0.69	17.90
HM-2400	4.8	26.1	68.1	1.0	76.95	3.32	0.74	18.99
HM-2700	2.7	25.0	71.3	1.0	78.54	3.25	0.59	17.62

Considering the ultimate analysis of both feedstocks, the carbon content weight percentage vastly increased after pyrolysis, while both hydrogen and oxygen content decreased. For softwood, the carbon weight percentage increased by about 42%, while hydrogen and

oxygen weight percentages decreased between 38.2-40.1% and 61.2-65.9%, respectively. Hemp biochar analysis follows identical trends with that of softwood data, with a 42.3-43.4% increase in carbon content after pyrolysis and 46.1-47.7% and 61.4-64.2% reduction in hydrogen and oxygen content, respectively. Similar results are well-documented [23], owing to the rapid release of volatiles during pyrolysis which escape as gas containing CO_2, CO, CH_4, and H [20]. Comparing the two biochar studied, there is little variance in elemental weight composition between the microwave power levels, owing to the hour-long pyrolysis residence time which allows the majority of the volatiles exit. These concepts are further explored examining the FT-IR results of the chars and raw species in subsequent paragraph.

4.3.2 Fourier Transform Infrared Spectroscopy

Figure 4.3.2.1 shows the FT-IR spectra of raw softwood and hemp feedstocks. It is seen that both softwood and hemp display similar curves containing stretches and peaks at key points where specific chemical bonds are present. This is attributed to the fact that both correspond to lignocellulosic biomass of similar chemical composition. The larger stretch from 3600 to 3200 cm^{-1} is attributed to the O-H stretching, a characteristic peak of crystalline cellulose [37]. C-H stretching is found near 2850 to 2890 cm^{-1} and 700 to 800 cm^{-1} relating to aliphatic and aromatic compounds [36]. Carbon-dioxide (O=C=O) is also present near 2400 cm^{-1} [21]. The C=O peak at 1735 cm^{-1} is credited to the vibration of the carboxylic acids in hemicellulose [37], while the C=C stretching from 1600 to 1740 cm^{-1} is a characteristic of cellulose compounds [20]. A stretch from the presence of C-C aromatic rings occurs near 1435-1475 cm^{-1} [20]. C-O stretching and deformation is notable

at 1215 and 1060 cm^{-1}, while the stretching vibration near 1160 cm^{-1} from C-O-C functional group is associated with lignin [38]. The organic compounds and their associated functional groups referenced are presented in Table 4.3.2.1.

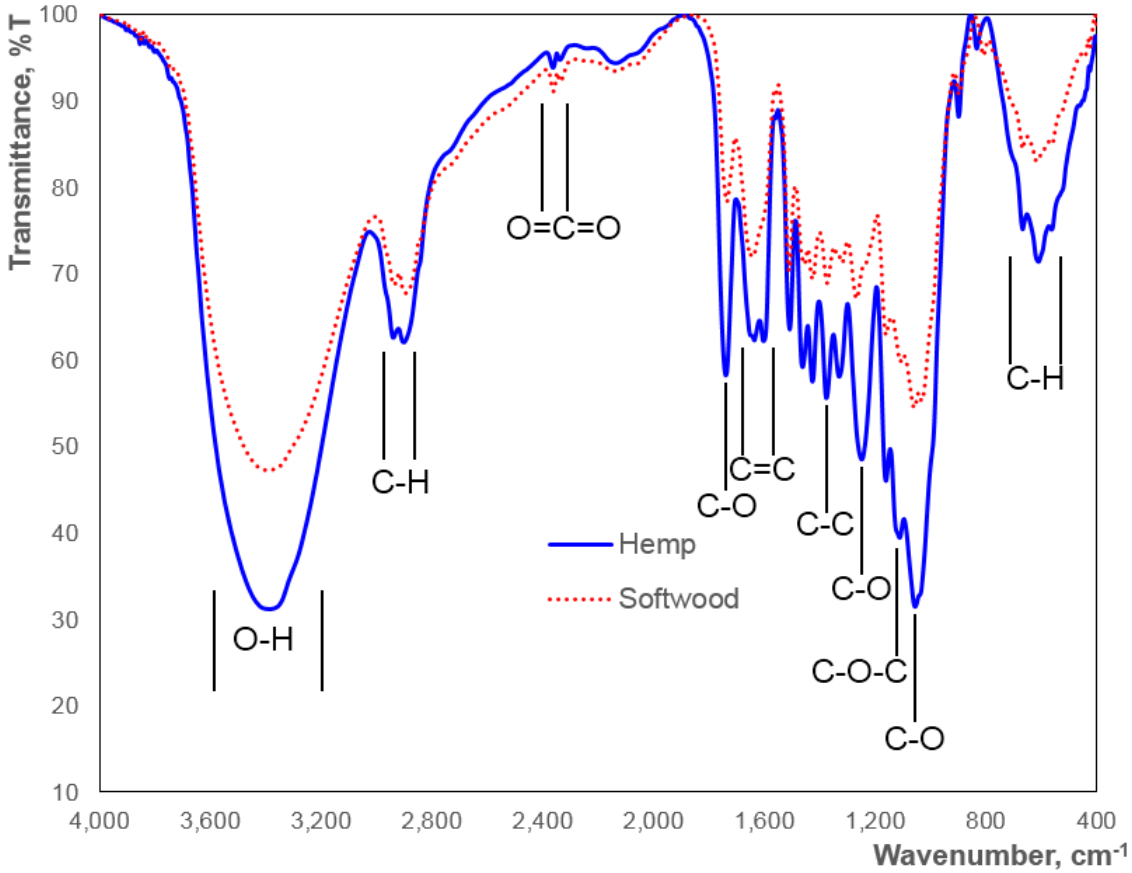

Figure 4.3.2.1: FT-IR spectra of raw softwood and hemp feedstocks

Table 4.3.2.1: Organic compounds and associated functional groups [20-21, 37-38]

Compound	Functional group	Wave number, cm^{-1}
Cellulose	O-H	3600-3200
	C=C	1600-1740
Hemicellulose	C=O	1735
Lignin	C-O-C	1160

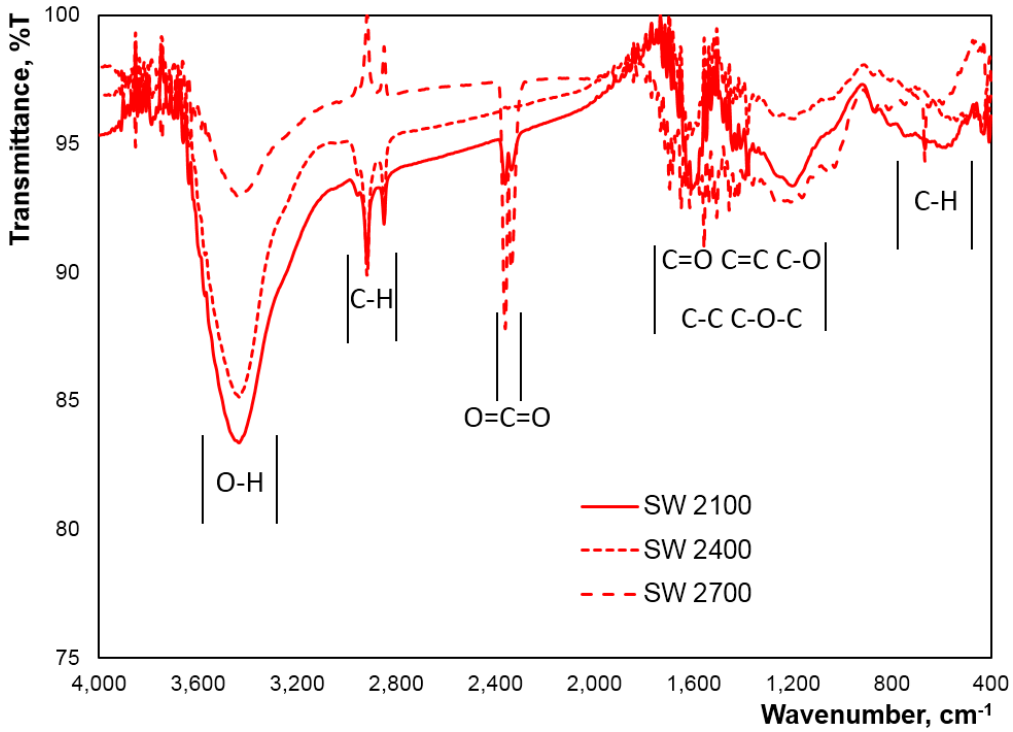

Figure 4.3.2.2: FT-IR spectra corresponding to softwood biochar as a function of microwave power level

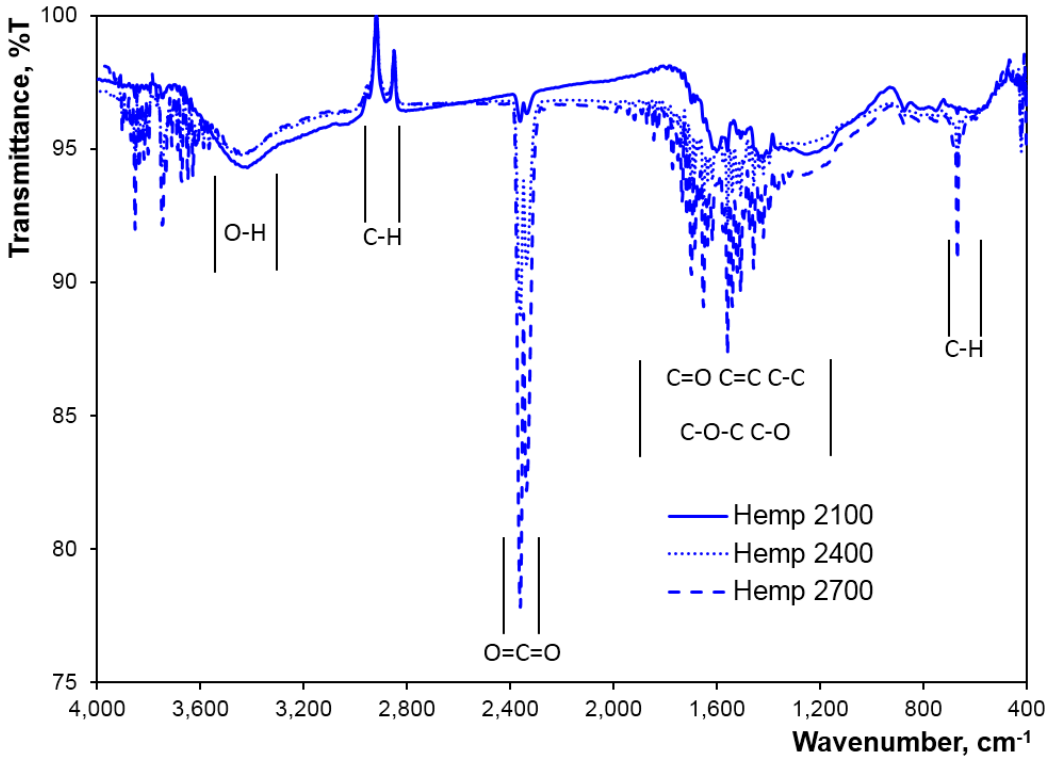

Figure 4.3.2.3: FT-IR spectra corresponding to hemp biochar as a function of microwave power level

Figures 4.3.2.2 and 4.3.2.3 display the FT-IR spectra corresponding to softwood and hemp biochars with respect to their individual microwave processing power. Across all spectra there is a major loss in transmittance of infrared radiation, most notably in the functional groups and compounds associated with lignocellulosic biomass. The large O-H stretch associated with cellulose experiences varying degrees of degradation between the power levels, with the largest being at 2700 Watt for both the woody and non-woody biomasses. The aliphatic and aromatic C-H compounds display different results, with the largest aliphatic loss occurring at 2700 Watt, and largest loss of aromatic occurring at 2100 Watt. These observations indicate that the individual compounds may degrade at separate rates based on the processing temperatures of pyrolysis. An increase in CO_2 transmittance occurs

as temperatures increase due to C=O bonds more readily breaking at elevated temperatures to form CO and CO_2 [21]. Major changes occur throughout the region from 700 to 1740 cm^{-1}, as the dehydration of hemicellulose and lignin lead to a loss of aliphatic C-H, C-O-C, and olefinic C=C groups. The loss of organic compounds during pyrolysis promoted a growth of organic chemical structures containing aromatic compounds as feedstock carbonized [20]. While each feedstock experiences similar loss of lignocellulosic compounds throughout pyrolysis, the spectra results show varying levels of loss based on processing temperatures, further proving that softwood and hemp biomasses have characteristic pyrolysis conditions for production of quality biochar [37].

4.4 Biochar structural properties

4.4.1 Scanning electron microscopy images

Figure 4.4.1.1 shows the SEM images of SW-2100 (A), SW-2400 (B), SW-2700, (C) HM-2100 (D), HM-2400 (E), and HM-2700 (F) samples. These secondary SEM images were taken at 2000x magnification to examine the structural morphology. Evidently, each sample exhibited a porous structure including pore size, shape, and their distribution. Comparing Softwood (A, B, C) with Hemp (D, E, F) biochar samples it is clear that softwood biochar contains larger pore size, while the hemp biochar has the presence of higher volume of smaller pores. Further, as power level increased there is less evidence of pore cracking and residual tars present inside the pores for both softwood and hemp samples. This observation can be attributed to a more rapid release of volatiles during the increased heating rates at corresponding power levels, leaving to larger and healthier pores [7].

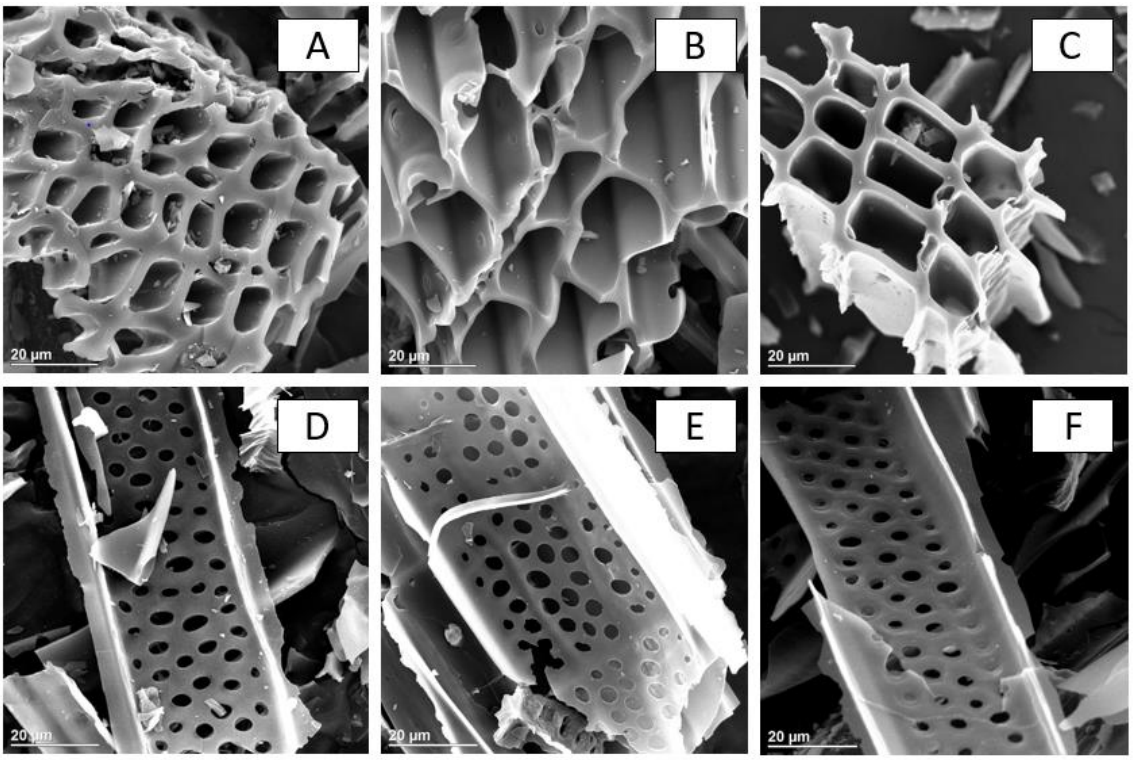

Figure 4.4.1.1: SEM images of softwood (A, B, C) and hemp (D, E, F) biochar

4.4.2 BET surface area and porosity analysis

The physiosorption analysis provided in Table 4.4.2.1 include found porosity characteristics of the raw hemp and softwood samples. Comparing these raw samples to the biochar indicates a large increase BET surface area after pyrolysis. Most notably the raw feedstocks have no applicable micropores, while new micropores were developed in the char during pyrolysis. For both feedstock types, porosity results, including BET surface area and micropore area, improved as power level increases from 2100 watts to 2400 watts, owing to the faster rate of residual volatile release, and increased development of micropores at the elevated heating rates [8, 21]. This occurrence is often stronger in

microwave pyrolysis over conventional as the microwaves heighten tar vaporization lending to faster release of volatiles, opening clearer pores [39]. Further indication of micropore development is the large decrease in average pore diameter from comparison of the raw feedstock to their biochars, and the 2100 watt chars to the 2400 watt chars.

Table 4.4.2.1: Physiosorption analysis results

Sample	BET Surface Area (m^2/g)	Average Pore Diameter (Å)	Micropore Area (m^2/g)	Average Pore Volume (cm^3/g)
Hemp	2.97	78.06	N/A	0.0058
Softwood	0.76	134.86	N/A	0.0026
SW - 2100W	14.44	40.52	4.89	0.0146
SW - 2400W	28.65	30.53	16.07	0.0219
SW - 2700W	9.96	46.44	1.63	0.0116
HM - 2100W	11.72	65.34	0.75	0.0191
HM - 2400W	12.26	59.65	2.97	0.0183
HM - 2700W	12.18	52.75	2.58	0.0161

Considering the physiosorption results from 2400 to 2700 watt for both biochars, the BET surface area and micropore area reduces, with a larger decline for softwood char than hemp char. This phenomenon has been previously reported, with surface pore size of biochars decreasing with increased pyrolysis temperature, explained as the potential for biochar to melt and deform causing pores to shrink or potentially close at elevated temperatures [40]. Deformation or melting of the biochar could have indeed occurred for the 2700 watt experiments considering the large recorded residence temperatures of biochar production, 600 °C and 650 °C for hemp and softwood respectively. Considering the recorded results it is reasonable to conclude there may be optimal temperature conditions for biochar production, which is under 600 °C.

4.5 Biochar mechanical properties

Material Young's modulus and hardness properties are the measures for its ductility and strength behavior. When it comes to biochar particles since many of its applications are targeting it to be as filler material it is imperative that these properties are evaluated at their nano-scale. Figure 4.5.1 shows the comparative nanohardness and Young's modulus properties of both softwood and hemp char particles.

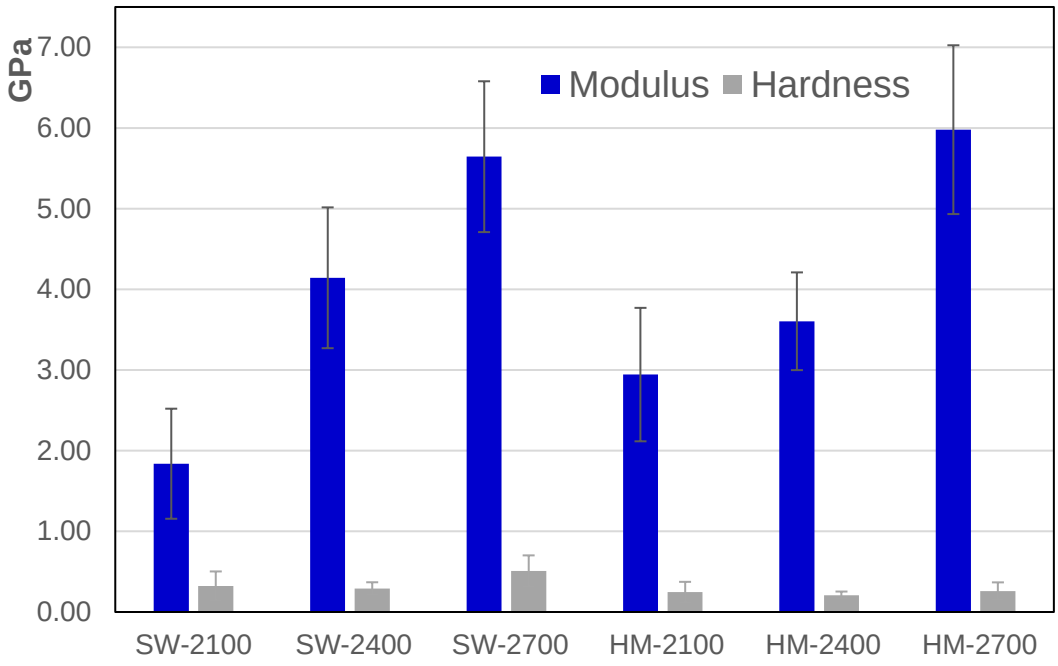

Figure 4.5.1: Hardness and Young's modulus values for biochars at different power levels

The hardness values for both softwood and hemp biochars remained virtually unchanged throughout the power level variations, 0.35 GPa for the former and 0.24 GPa for the latter. This could be due to the hour-long pyrolysis processing, as well as similar weight percentages of hard carbon element present, as reported in Table 5 ('Ultimate analysis'

results). On the other hand, the modulus values are found to increase with power level increment, with the peak values resonating at 5.64 GPa and 5.98 GPa for respective softwood and hemp biochars, processed at 2700 Watt. Similar data were recorded on biochar originating from pine sawdust, another softwood species [24, 25]. It was hypothesized that pyrolysis heating rate and temperature are the most significant indicators of underlying mechanical properties when it comes to biochar particles. This is explained due to the presence of residual pyrolytic tars and carbon molecules at lower processing temperatures, resulting in lower hardness and Young's modulus [41]. Furthermore, as heating rate increases these volatiles exit the char at a faster rate, promoting the growth of healthy pores resulting in added strength in char particles [8]. This is apparent when comparing the higher peak modulus of hemp to softwood and their corresponding heating rates. Further explanation for this upward trend observed is given as a gradual transition from a visco-plastic biomaterial into a brittle, glass-like carbonaceous residue at temperatures above 400^{o}C [41]. This discussion is further reinforced linking with biochar elastic behavior under the load-depth curve, as shown in Figures 4.5.2 and 4.5.3.

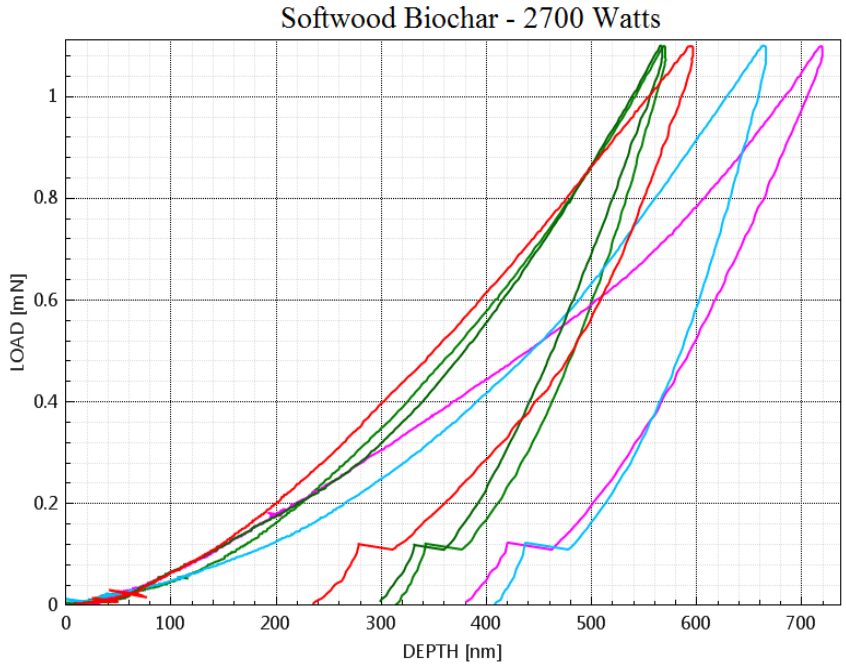

Figure 4.5.2: Elastic behavior of softwood biochar particles at 2700 Watts

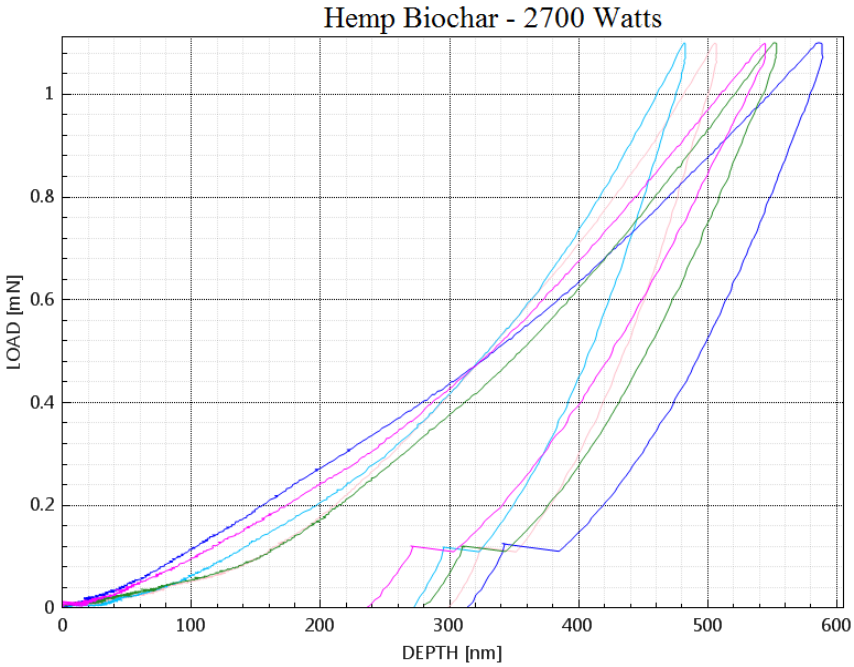

Figure 4.5.3: Elastic behavior of hemp biochar particles at 2700 Watts

Comparing these two feedstocks, it is noted that while the curves take similar shapes, the average recovery of penetration depth for the hemp sample is slightly larger compared to that of the softwood sample, owing to the higher elasticity associated non-woody biomass. This is an important finding for them to be utilized in the biocomposites manufacturing and gain flexural strength properties.

4.6 Biocomposites Mechanical Testing Results

4.6.1 Flexural Testing

Unidirectional fiber reinforced composites are characteristically strong in tension due to the high tensile strength of the fiber reinforcements. As flexural strength is a more elaborate property, with dependence on both tensile and compressive regions, many unidirectional pultruded composites are much weaker in flexure than tension, relying on the weaker matrix for support in the compression region of flexural bending. Adding biochar as a particulate filler provides opportunity to improve the flexural strength of the overall biocomposites as the hard, porous particles contribute to a more elaborate and stiffer biocomposites matrix [4, 42]. To further investigate the benefit of biochar as a reinforcing filler, three-point bending tests were performed six times and statistically averaged for each biocomposites sample, as well as the control samples lacking biochar. While three-point bending failure still occurred in the compressive region for all samples, the results displayed in Figure 4.6.1.1 reinforce the theory the biochar provides strong support in the compressive region, and increases the overall flexural strength of the biocomposites.

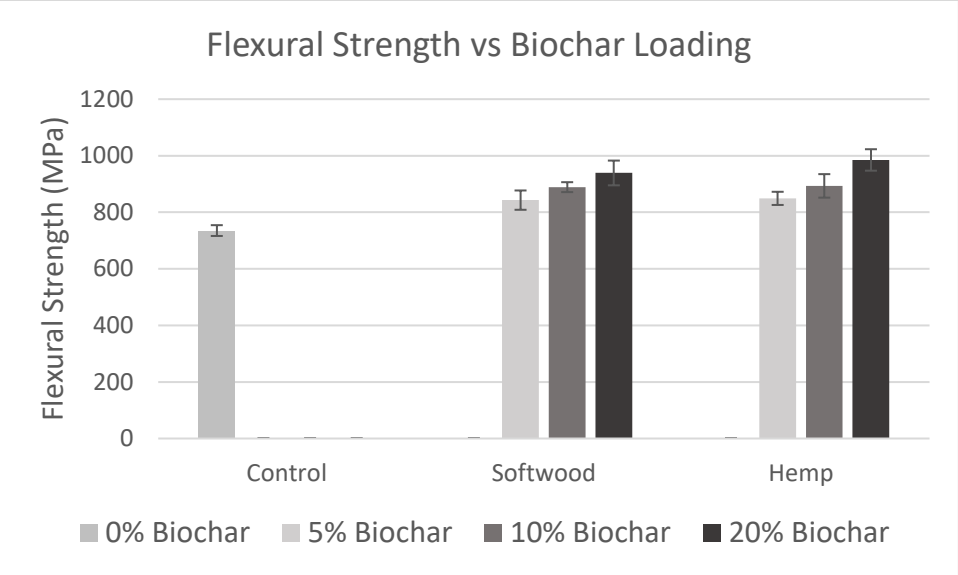

Figure 4.6.1.1: Flexural strength results

Table 4.6.1.1 summarizes the averaged flexural strength values and percentage of strength increase found through three-point bending of the control and biocomposites rods. It is important to note that the flexural strength increase is not linear with increased biochar addition. As higher volume percentages of biochar is added to the matrix mixture, the bonding strength of the overall composite may decrease owing to a reduction of interfacial bonding between the matrix and reinforcements as resin volume fraction decreases [43].

Table 4.6.1.1: Flexural strength results with percentage increase

Composite	Flexural Strength (MPa)	Percent Increase (%)
Control	735 ± 19	-
Sw_5	843 ± 34	14.6
Sw_10	889 ± 18	20.9
Sw_20	939 ± 44	27.7
Hm_5	849 ± 23	15.5
Hm_10	893 ± 42	21.5
Hm_20	985 ± 38	34.0

Flexural modulus of the biocomposites was found from analysis of the stress-strain curves generated from three-point bending. Figure 4.6.1.2 displays the averaged modulus of each biocomposites and control rods for comparison. For both softwood and hemp biochar reinforced biocomposites, flexural modulus increased as biochar volume percentage increased, the maximum increase was 6.5% from 20% hemp biochar addition. While it is well known that the inclusion of hard particles to the matrix of unidirectional fiber composites will increase the flexural strength [43] it is important to acknowledge the role of the higher young's modulus of the biochar introduced to the softer vinyl ester resin matrix. Notably, the hemp biochar biocomposites performed better in flexure and had a similar or higher experimental flexural modulus than the softwood char biocomposites, while also having a higher individual experimental modulus found during nanoindentation (Figure 4.5.1), as well as being significantly more porous than the softwood samples (Table 4.4.2.1).

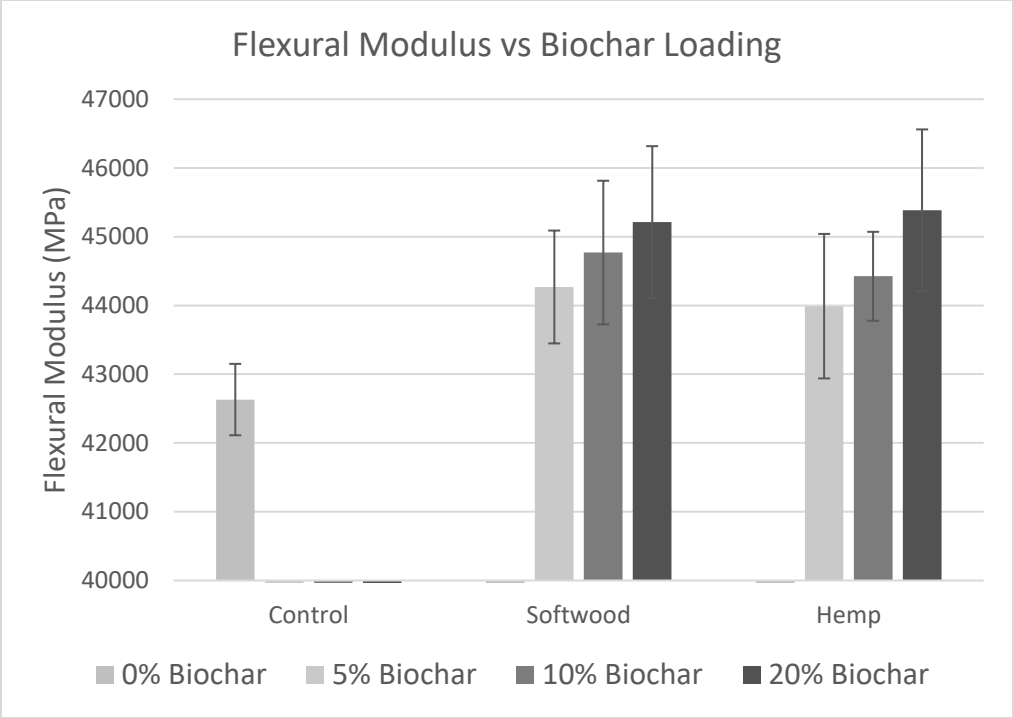

Figure 4.6.1.2: Flexural modulus results

Table 4.6.1.2: Comparison of experimental and Rule of Mixtures flexural modulus

Biocomposites	Experimental Modulus (GPa)	RoM Modulus (GPa)	Percent Difference (%)
Control	42.63 ± 0.52	46.48	9.03
Sw_5	44.26 ± 0.82	46.52	5.11
Sw_10	44.76 ± 1.44	46.57	4.04
Sw_20	45.21 ± 1.10	46.66	3.21
Hm_5	43.98 ± 1.05	46.53	5.79
Hm_10	44.42 ± 0.64	46.58	4.86
Hm_20	45.38 ± 1.17	46.69	2.89

Table 4.6.1.2 contains rule of mixtures calculations for flexural modulus of the biocomposites. Hemp biochar biocomposites were found to have a higher theoretical flexural modulus owing to the larger modulus of the hemp biochar, while this was actually

true for the 20% biochar samples, the theoretical results were not as aligned to experimental for the 5, and 10% samples. Considering the percentage differences between the experimental and rule of mixtures results, it is apparent that while the rule of mixtures model is somewhat effective at predicting the flexural modulus, it over predicts from the actual modulus. Rule of mixtures calculations are often considered to be the upper-bounds estimate of the composite modulus, as it does not take into consideration composite defects such as bonding or voids [44].

4.6.2 Tensile Testing

Tensile testing was performed three times on each biocomposites sample type, with load data collected through load cells in the Instron Universal Testing machine and strain data collected through an Instron clip-on extensometer for two tests, and digital image correlation technique for one test per biocomposites sample. A tensile stress-strain curve found through DIC tensile testing of the 20% Softwood biocomposites type is presented in Figure 4.6.2.1 along with some digital images collected and analyzed throughout the test. The resulting curve presents a linear increase of strain as the loading increased (A through C) until fracture (D). These results are expected and follow the conventional glass-fiber reinforced polymer curves as the majority of strain during longitudinal loading is held in the reinforcing fibers rather than matrix [45]. Failure of the biocomposites was characterized by initial single fiber failures followed by violent reaction as the remaining fibers collectively failed from the increased stress.

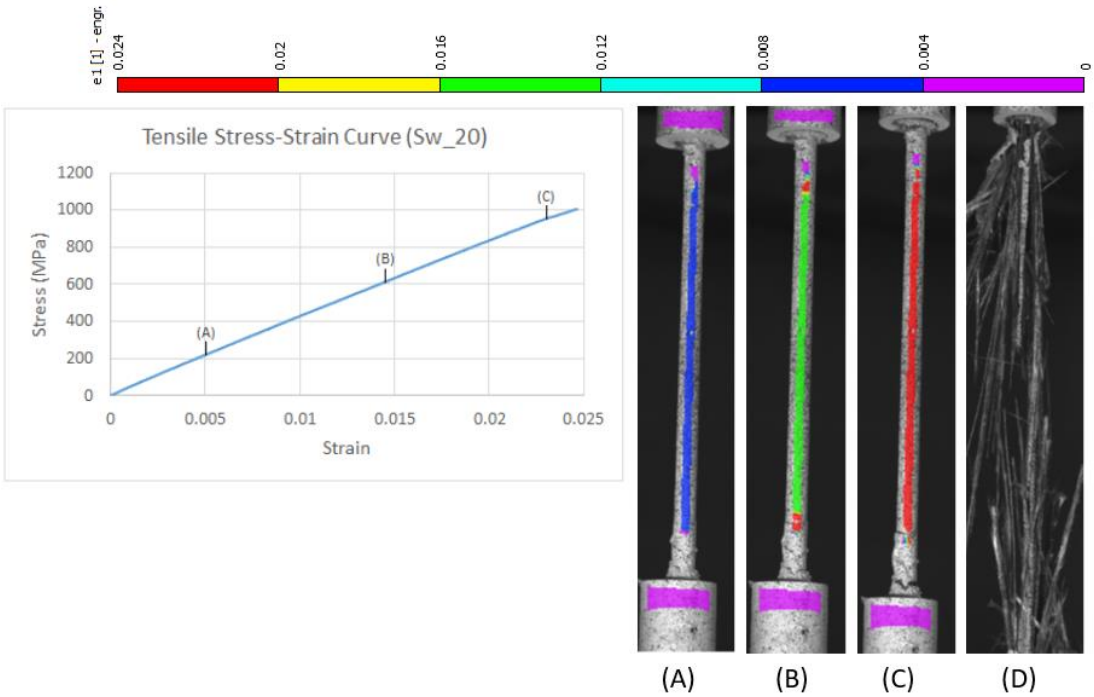

Figure 4.6.2.1: Digital Image Correlation results from tensile testing

The averaged tensile stress results displayed in Figure 4.6.2.2 indicate that while the addition of biochar increased the ultimate strength, there is no significant relationship between amount of biochar addition and increase of strength. While it has been stated that the majority of tensile stress is held in the fibers, the increase of yield strength is explained from the addition of biochar to the GFRP matrix creating a more elaborate matrix from which to hold some of the tensile stress during longitudinal loading [26]. Overall maximum increases in tensile strength were 10.1% increase from softwood biochar addition, and 12.5% from hemp addition compared to that of the control rebar [46].

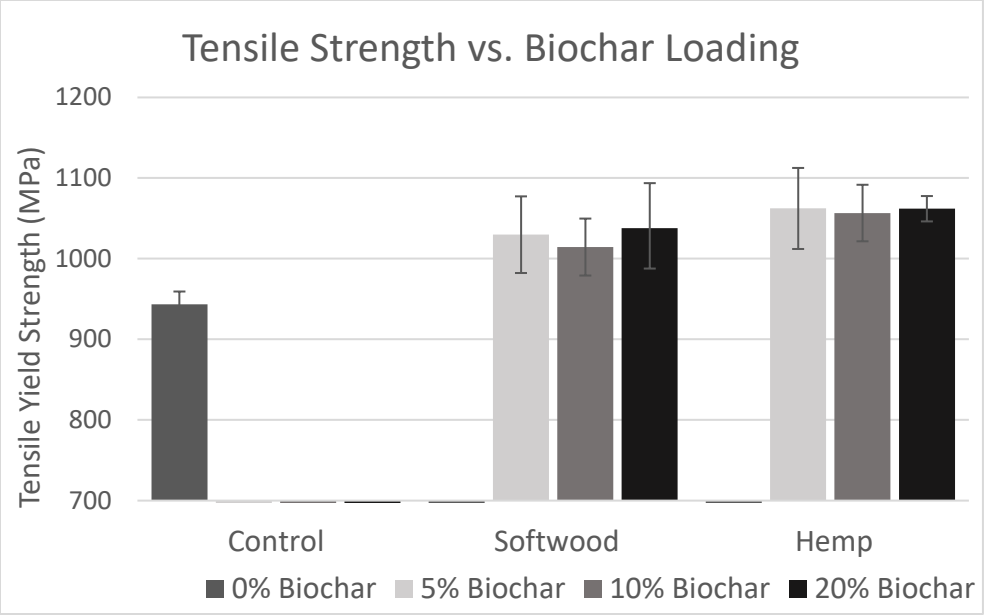

Figure 4.6.2.2: Tensile strength results

Considering the experimental tensile modulus results presented in Figure 15 there is small significance in change of modulus from the addition of biochar to the resin matrix. The highest increase is noted at 10% volume addition for each biochar species. The small increase of composite tensile modulus with biochar addition is again due to the influence of the stiff reinforcing-fibers contributing the majority of resistance to deformation. Studies on the composite matrix, combining neat polypropylene and biochar report that biochar addition can increase the overall tensile modulus due to enhanced stress transfer properties between the polypropylene and stiffer biochar from mechanical interlocking [47]. Mechanical interlocking is described to occur when the molten polypropylene flows through the porous char, creating a stronger matrix upon curing [47]. The results in Figure 4.6.2.3 also indicate a decline in tensile modulus from 10% to 20% volume addition of biochar to the matrix. As the biochar load increases, concern on the quality of interfacial

bonding arises, due to potential agglomeration of particles inside the matrix decreasing overall bonding strength [43].

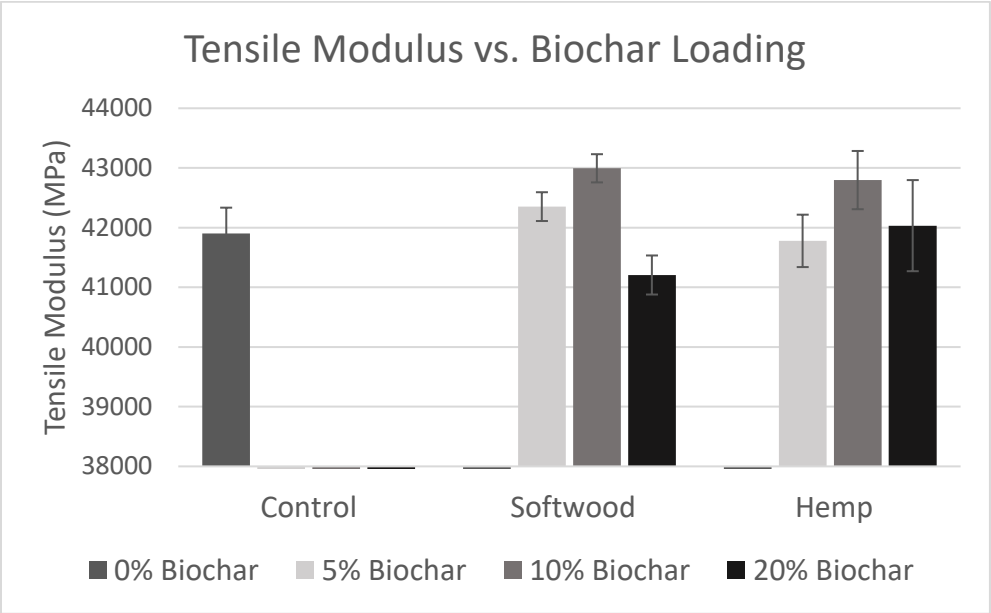

Figure 4.6.2.3: Tensile modulus results

Comparing the rule of mixtures calculations with experimental tensile results in Table 4.6.2.1 indicates a somewhat large percent difference (8.05 to 13.11 %) between the composites and model. As stated earlier, the rule of mixtures is considered an upper-bounds limit of the modulus found through ideal conditions and neglecting composite defects such as voids or non-perfect bonding [44]. Additionally from comparison of the control rod results with the rule of mixtures it can be argued that there may be additional defects in the fibers themselves which have had a lengthy storage-life.

Table 4.6.2.1: Comparison of experimental and Rule of Mixtures tensile modulus

Biocomposites	Experimental Modulus (GPa)	RoM Modulus (GPa)	Percent Difference (%)
Control	42.24 ± 0.89	46.40	9.85
Sw_5	42.35 ± 0.24	46.45	8.05
Sw_10	42.99 ± 0.23	46.50	8.16
Sw_20	41.20 ± 0.33	46.60	13.11
Hm_5	41.71 ± 0.54	46.46	11.39
Hm_10	42.80 ± 0.49	46.51	8.67
Hm_20	41.90 ± 0.76	46.63	11.29

4.7 Finite Element Analysis and Modeling

Figure 4.7.1 displays visual stress results in the z-direction from the Abaqus simulation of the biochar-resin matrix model. Owing to the assumed spherical shape of the particles and isotropic nature of the vinyl-ester resin, young's modulus is the same is each direction. The homogenized modulus found through FEA simulation is compared to the rule of mixtures calculated modulus in Table 4.7.1.

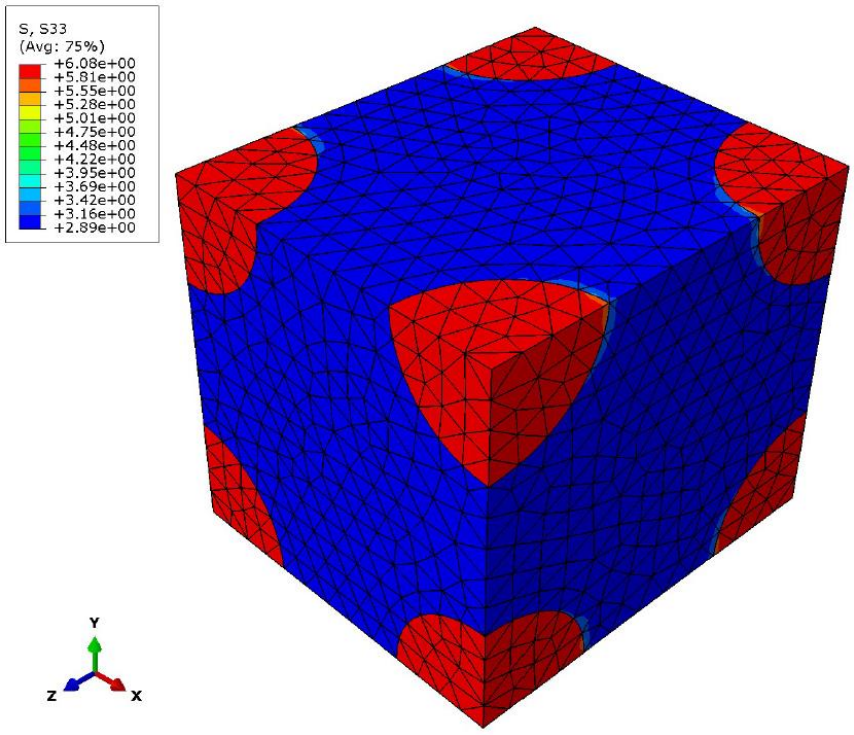

Figure 4.7.1: Abaqus particle-matrix stress results

Table 4.7.1: Comparison of FEA and Rule of mixtures particle-matrix results

Biochar/Resin Model	FEA Modulus (GPa)	Rule of Mixtures Modulus (GPa)	Percent Difference (%)
Sw_5	3.132	3.132	0.0
Hm_5	3.149	3.149	
Sw_10	3.266	3.264	0.06
Hm_10	3.3	3.298	
Sw_20	3.532	3.528	0.11
Hm_20	3.6	3.596	

Evaluating the finite element analysis models versus the rule of mixtures calculations in Table 4.7.1 indicates a very small percentage of difference between the two micromechanical modeling techniques. The close similarity between the findings from the

two techniques is due to the fact that both models are built off of the same assumptions of perfect bonding between the matrix and inclusions, and hard spherical biochar particles. Larger difference in models, and more accurate homogenization modeling could be found through accounting for the biochar porosity characteristics. Percentage of difference between the FEA modulus and rule of mixtures calculations was found to be the same for each biochar loading percentage as the same model was used for each test, while changing the material properties in the simulation.

Figure 4.7.2 displayed the visual stress results due to simulation of uniform strain in the fiber-direction of the biocomposites representative volume element. As the fiber reinforcements have the highest tensile strength of the three constituents, the majority of stress is held in the fibers. Table 4.7.2 contains the homogenized modulus along the fiber direction for each biocomposites type, compared to the rule of mixtures model calculations.

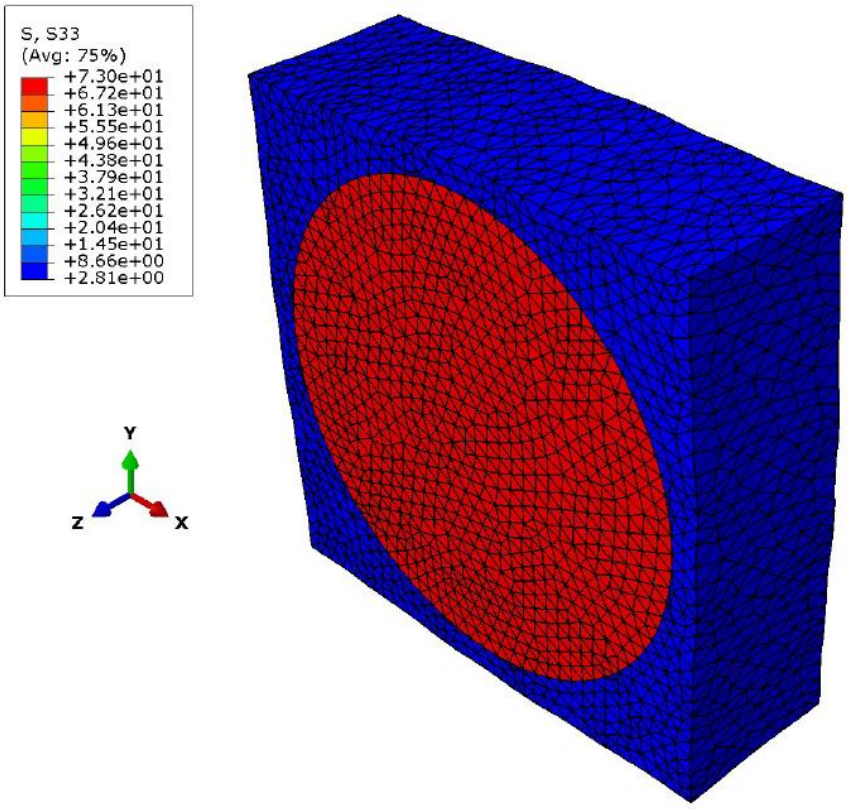

Figure 4.7.2: Abaqus composite stress results

Table 4.7.2: Comparison of FEA and Rule of mixtures composite results

Biocomposites	FEA Modulus (GPa)	Rule of Mixtures Modulus (GPa)	Percent Difference (%)
Control	46.417	46.400	0.04
Sw_5	46.465	46.450	0.03
Hm_5	46.519	46.500	
Sw_10	46.628	46.601	0.04
Hm_10	46.472	46.457	
Sw_20	46.532	46.513	0.06
Hm_20	46.656	46.626	

Modulus (E_{11}) values for the biocomposites in the fiber direction closely align when found through each micromechanical model, with the largest percent difference being 0.06%. Again, this is because both models are based off of the same assumptions. When comparing the micromechanical modeling results to the experimental results found through tensile testing in Table 4.7.3, it is apparent that both models far overestimate the tensile modulus of the biocomposites. Explanations owing to the ideal assumptions of the models compared to potential defects of the composites have been stated throughout this study. The FEA model could also further be improved through advanced modeling of the porous properties of the biochar and flow of the resin through said pores. It is further noted that results may improve by adopting a model that better represents the randomness of the biochar particle distribution inside the resin matrix [45].

Table 4.7.3: Comparison of experimental and FEA composite results

Biocomposites	Experimental Modulus (GPa)	FEA Modulus (GPa)	Percent Difference (%)
Control	42.24 ± 0.89	46.417	9.89
Sw_5	42.35 ± 0.24	46.465	9.72
Hm_5	42.99 ± 0.23	46.519	8.21
Sw_10	41.20 ± 0.33	46.628	13.17
Hm_10	41.71 ± 0.54	46.472	10.25
Sw_20	42.80 ± 0.49	46.532	8.72
Hm_20	41.90 ± 0.76	46.656	11.35

Chapter 5

Conclusions and Recommendations

5.1 Conclusions

The following conclusions have been made based on the data collected and discussed in this study:

1. Microwave pyrolysis of large batch required high microwave power levels (> 2000 Watt) to reach the needed pyrolysis temperatures (> 300^{o}C).
2. Pyrolysis heating rates for large batch sizes are low, ranging 25-50^{o}C/min, due to the amount of biomass the microwaves must penetrate.
3. Biochar yield was achieved up to 40 wt.% of the raw biomass, and volatile matter content decreased to as low as 33 wt.%, as heating rates increased due to faster release of bio-oil and bio-gas from the system.
4. Softwood and hemp biochars have similar elemental weight percentages after pyrolysis as they both came from lignocellulosic feedstocks.
5. With the power level increase the pores showed higher structural integrity, in terms of cracking and residual tars present inside them for both softwood and hemp samples.
6. Porosity results displayed an increase of BET surface area and micropore area from pyrolysis, owing to the rapid release of volatiles and development of new micropores relating to the heating rates of pyrolysis.

7. A decline in porosity results at elevated microwave power levels (2700 watts), indicated an optimal production temperature under 600 °C, owing to the shrinkage and deformation of pores at elevated temperatures.
8. Both softwood and hemp samples showed higher Young's modulus (5.64 GPa vs. 5.95 GPa, respectively) with the increase in pyrolysis temperatures, the maximum being 2700 Watt. This is due to the decrease in the residual volatiles and increase in the fixed carbon content upon pyrolysis at elevated temperatures (>300^{o}C).
9. The mechanical load-depth behavior from the nanoindentation tests indicated the 'quasi' elastic behavior of the biochar particles, an important finding for them to be utilized in the biocomposites manufacturing and gain flexural strength properties. Therefore, upon comprehensive mechanical tests of these biocomposites materials under 3-point bend tests the potential for biochar as a composite filler material in high-strength application is promising.
10. The addition of biochar as a reinforcing filler to the matrix of GFRP composites significantly increases the flexural strength of the biocomposites (up to 34% at 20% hemp biochar volume loading)
11. The addition of biochar also significantly increases the flexural modulus of the biocomposites rods (up to 6.5% at 20% hemp biochar volume loading).
12. As shown when comparing the hemp and softwood biocomposites, main factors for the potential increase of flexural properties is the biochar modulus and porosity, owing to the mechanical interlocking of the biochar/resin creating a stiffer matrix.
13. The addition of biochar increased the tensile strength of the biocomposites by creating an elaborate matrix for bonding (Up to 12.5% at 20% hemp biochar volume loading)

14. The addition of biochar does not significantly change the biocomposites tensile modulus as the majority of stress is held in the stiff fibers during tensile loading.
15. Hemp biochar was found to be more beneficial for biocomposites manufacturing than softwood owing to the greater modulus and porosity/surface area characteristics.
16. Micromechanical models can be used with some success for this novel three-part composite but overestimate the composite properties due to the ideal-case assumptions of these models.

5.2 Recommendations

Based on the results and conclusions of this study, there is strong potential for the use of biochar as a reinforcing filler in pultruded fiber reinforced polymers. The following future work is suggested in order to further the understanding and potential of these novel biocomposites:

1. Develop a wider-array of experiments pertaining to the effects of biochar as an additive filler in the biocomposites. Most importantly would be the effects of varying particles size as larger particles may increase the flexural strength of the biocomposites or might have negative effects due to a reduction in quality of interfacial bonding between the constituents.
2. Perform more comprehensive testing of the biocomposites pertaining to their potential uses in industry. This would include compressive and fatigue loadings for mechanical strength, as well as testing of the biocomposites chemical properties. Glass-fiber reinforced composites are known to be noncorrosive as well as having

beneficial thermal qualities, the biocomposites will need to be tested to understand the effects of biochar on these properties prior to industrial use.

3. A more advanced finite element analysis model should be developed in order to better predict the mechanical properties of the biocomposites under various loading conditions. In this study the developed model had between 8 to 13 percent difference in tensile modulus from the experimental data. An advanced model would take into consideration the porous properties of the biochar as well as the randomness of the biochar particle distribution.

Bibliography

[1] Basu, P. (2013). *Biomass gasification, pyrolysis and torrefaction: Practical design and theory*. Amsterdam: Academic Press.

[2] Das, O., Bhattacharyya, D., & Sarmah, A. K. (August 15, 2016). Sustainable eco-composites obtained from waste derived biochar: a consideration in performance properties, production costs, and environmental impact. Journal of Cleaner Production, 129, 159-168.

[3] Das, O., Sarmah, A. K., & Bhattacharyya, D. (April 15, 2015). A sustainable and resilient approach through biochar addition in wood polymer composites. *Science of the Total Environment, 512.*

[4] Das, O., Bhattacharyya, D., Hui, D., & Lau, K.-T. (December 01, 2016). Mechanical and flammability characterizations of biochar/polypropylene biocomposites. *Composites Part B, 106*, 120-128.

[5] Li, J., Dai, J., Liu, G., Zhang, H., Gao, Z., Fu, J., et al. (2016). Biochar from microwave pyrolysis of biomass: A review. *Biomass and Bioenergy* (94), 228-244.

[6] Luque, R., Ángel Menéndez, J., Arenillas, A., & Cot, J. (2012). Microwave-assisted pyrolysis of biomass feedstocks: the way forward? *Energy Environ. Sci , 5* (2), 5481-5488.

[7] Salema, A., Afzal, M., & Bennamoun, L. (2017). Pyrolysis of corn stalk biomass briquettes in a scaled-up microwave technology. *Bioresource Technology, 233*, 353-362.

[8] Mašek, O., Budarin, V., Gronnow, M., Crombie, K., Brownsort, P., Fitzpatrick, E., & Hurst, P. (March 01, 2013). Microwave and slow pyrolysis biochar—Comparison of physical and functional properties. *Journal of Analytical and Applied Pyrolysis, 100*, 41-48.

[9] Fernandez Y, Arenilllas A, Mendendez A. *Microwave Heating Applied to Pyrolysis.* Instituto Nacional Del Carbon, Oviedo, Spain

[10] Daniel, I. M., & Ishai, O. (1994). *Engineering mechanics of composite materials*. New York: Oxford University Press.

[11] Gobinda S. *Experimental, Numerical, and Analytical Studies of Smart Composite Materials and Their Applications (PhD Thesis).* Dalhousie University, Halifax, Nova Scotia, 2005

[12] Das, O., Hedenqvist, M. S., Kim, N. K., Lin, R. J. T., Bhattacharyya, D., & Sarmah, A. K. (March 28, 2018). An Attempt to Find a Suitable Biomass for Biochar-Based Polypropylene Biocomposites. *Environmental Management,* 1-11.

[13] Huang, Y.-F., Chiueh, P.-T., Kuan, W.-H., & Lo, S.-L. (August 01, 2013). Microwave pyrolysis of rice straw: Products, mechanism, and kinetics. *Bioresource Technology, 142,* 620-624.

[14] Huang, Y.-F., Chiueh, P.-T., Kuan, W.-H., & Lo, S.-L. (April 01, 2016). Microwave pyrolysis of lignocellulosic biomass: Heating performance and reaction kinetics. *Energy, 100,* 137-144.

[15] Liu, H., E, J., Deng, Y., Xie, C., & Zhu, H. (August 05, 2016). Experimental study on pyrolysis characteristics of the tobacco stem based on microwave heating method. *Applied Thermal Engineering, 106,* 473-479.

[16] Zhao, X., Wang, M., Liu, H., Zhao, C., Ma, C., & Song, Z. (March 01, 2013). Effect of temperature and additives on the yields of products and microwave pyrolysis behaviors of wheat straw. Journal of Analytical and Applied Pyrolysis, 100, 49-55.

[17] Yu, F., Steele, P. H., & Ruan, R. (January 04, 2010). Microwave Pyrolysis of Corn Cob and Characteristics of the Pyrolytic Chars. *Energy Sources, Part A: Recovery, Utilization, and Environmental Effects, 32,* 5, 475-484.

[18] Hossain, M. A., Ganesan, P. B., Sandaran, S. C., Rozali, S. B., & Krishnasamy, S. (January 01, 2017). Catalytic microwave pyrolysis of oil palm fiber (OPF) for the biochar production. *Environmental Science and Pollution Research International, 24,* 34, 26521-26533.

[19] Mohamed, B. A., Kim, C. S., Ellis, N., & Bi, X. (January 01, 2016). Microwave-assisted catalytic pyrolysis of switchgrass for improving bio-oil and biochar properties. *Bioresource Technology, 201,* 121-32.

[20] Zhu, L., Lei, H., Wang, L., Yadavalli, G., Zhang, X., Wei, Y., Liu, Y., Ahring, B. (September 01, 2015). Biochar of corn stover: Microwave-assisted pyrolysis condition induced changes in surface functional groups and characteristics. *Journal of Analytical and Applied Pyrolysis, 115,* 149-156.

[21] Zhao, X., Wang, M., Liu, H., Li, L., Ma, C., & Song, Z. (January 01, 2012). A microwave reactor for characterization of pyrolyzed biomass. *Bioresource Technology: Biomass, Bioenergy, Biowastes, Conversion Technologies, Biotransformations, Production Technologies, 104,* 673-678.

[22] Xian-Hua, W., Han-Ping, C., Xue-Jun, D., Hai-Ping, Y., Shi-Hong, Z., & Ying-Qiang, S. (August 01, 2009). Properties of gas and char from microwave pyrolysis of pine sawdust. *Bioresources, 4,* 3.)

[23] Huang, Y. F., Kuan, W. H., Lo, S. L., & Lin, C. F. (November 01, 2008). Total recovery of resources and energy from rice straw using microwave-induced pyrolysis. *Bioresource Technology, 99,* 17, 8252-8258.

[24] Das, O., Sarmah, A. K., & Bhattacharyya, D. (January 01, 2015). Structure-mechanics property relationship of waste derived biochars. *The Science of the Total Environment, 538,* 611-20.

[25] Das, O., Sarmah, A. K., & Bhattacharyya, D. (April 15, 2016). Nanoindentation assisted analysis of biochar added biocomposites. *Composites Part B, 91,* 219-227.

[26] Ogunsona, E. O., Misra, M., & Mohanty, A. K. (January 20, 2017). Sustainable biocomposites from biobased polyamide 6,10 and biocarbon from pyrolyzed miscanthus fibers. *Journal of Applied Polymer Science, 134,* 4.)

[27] Bowlby, L. K., Saha, G. C., & Afzal, M. T. (July 01, 2018). Flexural strength behavior in pultruded GFRP composites reinforced with high specific-surface-area biochar particles synthesized via microwave pyrolysis. *Composites Part A, 110,* 190-196.

[28] Kalamkarov, A. L., Hassan, E. M., Georgiades, A. V., & Savi, M. A. (January 01, 2009). Asymptotic homogenization model for 3D grid-reinforced composite structures with generally orthotropic reinforcements. *Composite Structures, 89,* 2, 186-196.

[29] De, M. R. Q., Ferreira, R. T. L., Donadon, M. V., & Guedes, J. M. (May 23, 2018). Elastic properties of unidirectional fiber-reinforced composites using asymptotic homogenization techniques. *Journal of the Brazilian Society of Mechanical Sciences and Engineering, 40,* 5.)

[30] Soden, P. D., Hinton, M. J., & Kaddour, A. S. (January 01, 1998). Lamina properties, lay-up configurations and loading conditions for a range of fibre-reinforced composite laminates. *Composites Science and Technology, 58,* 7, 1011-1022.

[31] Branca, C., Di, B. C., & Galgano, A. (July 01, 2017). Experimental analysis about the exploitation of industrial hemp (Cannabis sativa) in pyrolysis. *Fuel Processing Technology, 162,* 20-29.

[32] Grytten, F., Daiyan, H., Polanco-Loria, M., & Dumoulin, S. (2009). Use of digital image correlation to measure large-strain tensile properties of ductile thermoplastics. *Polymer Testing,* 28(6), 653-660.

[33] Smith, M. (2009). ABAQUS/Standard User's Manual, Version 6.9. Providence, RI: Simulia.

[34] Kalamkarov, A. L. (1992). Composite and Reinforced Elements of Construction. Wiley, Chichester.

[35] Potluri, R. (2018). Mechanical properties evaluation of t800 carbon fiber reinforced hybrid composite embedded with silicon carbide microparticles: A micromechanical approach. *Multidiscipline Modeling in Materials and Structures*, *14*(3), 589-608.

[36] G. Papazafeiropoulos, M. Muñiz-Calvente, E. Martínez-Pañeda. (March 2017) Abaqus2Matlab: a suitable tool for finite element post-processing. *Advances in Engineering Software*, 105, 9-16.

[37] Liu, Z., Han, G. (2015). Production of solid fuel biochar from waste biomass by low temperature pyrolysis, *Fuel*, 158, 159-165.

[38] Yang, H., Yan, R., Chen, H., Lee, D., Zheng, C. (2007) Characteristics of hemicellulose, cellulose and lignin pyrolysis, *Fuel*, 86, 1781-1788.

[39] Motasemi, F., & Afzal, M. (2013) A review on the microwave-assisted pyrolysis technique, *Renewable and Sustainable Energy Reviews*, 28, 317-330.

[40] Wang X-H, Chen H-P, Ding X-J, Yang H-P, Zhang S-H, Shen Y-Q. (2009) Properties of Gas and char from microwave pyrolysis of pine sawdust. *Bioresources Technology*, 4, 946-959.

[41] Zickler, G.A., Schöberl, T., Paris, O. (2006) Mechanical properties of pyrolysed wood: a nanoindentation study, *Philosophical Magazine*, 86, 1373-1386.

[42] Ogunsona, E. O., Misra, M., & Mohanty, A. K. (January 20, 2017). Sustainable biocomposites from biobased polyamide 6,10 and biocarbon from pyrolyzed miscanthus fibers. Journal of Applied Polymer Science, 134, 4.

[43] Asi, O. (2009). Mechanical properties of glass-fiber reinforced epoxy composites filled with Al2O3 particles. *Journal of Reinforced Plastics and Composites, 28*(23), 2861-2867.

[44] Bakis, C. E., & Ripepi, M. J. (2015). Transverse mechanical properties of unidirectional hybrid fiber composites. In X. Xiao, D. Liu, & A. Loos (Eds.), Proceedings of the American Society for Composites - 30th Technical Conference, ACS 2015 DEStech Publications.

[45] Potluri, R. (2018). Mechanical properties evaluation of t800 carbon fiber reinforced hybrid composite embedded with silicon carbide microparticles: A micromechanical approach. *Multidiscipline Modeling in Materials and Structures,* 14(3), 589-608

[46] Abou Niaj, Mahmoud. (2018) Flexural, compressive, and tensile properties of pultruded GFRP bars *(M.Eng. Report)*. University of New Brunswick, Fredericton, New Brunswick.

[47] Das O, Sarmah A, Bhattacharyya D. (2016). Biocomposites from waste derived biochars: mechanical, thermal, chemical, and morphological properties. *Waste Management*, 49, 560–70.

Appendices

Appendix A: Microwave Pyrolysis Experiment Data

Table A1: Softwood pyrolysis experiment data

Experiment #	Power Level (W)	Residence Temperature (°C)	Char (g)
SW 1	2100	350-400	429.16
SW 2	2100	350	426.14
SW 3	2100	300-380	343.7
SW 4	2400	400-450	304.99
SW 5	2400	400-500	273.66
SW 6	2400	350-450	327.75
SW 7	2700	600	246.49
SW 8	2700	600-650	227.52
SW 9	2700	600-700	235.6

Table A2: Hemp pyrolysis experiment data

Experiment #	Power Level (W)	Residence Temperature (°C)	Char (g)
H 1	2100	350-450	371.77
H 2	2100	300-400	350.95
H 3	2100	400-450	388.95
H 4	2400	430-530	305.7
H 5	2400	500-550	333.4
H 6	2400	500-570	356.02
H 7	2700	550-650	274.67
H 8	2700	550-650	285.76
H 9	2700	570-680	272.72

Appendix B: Temperature Profiles and Data

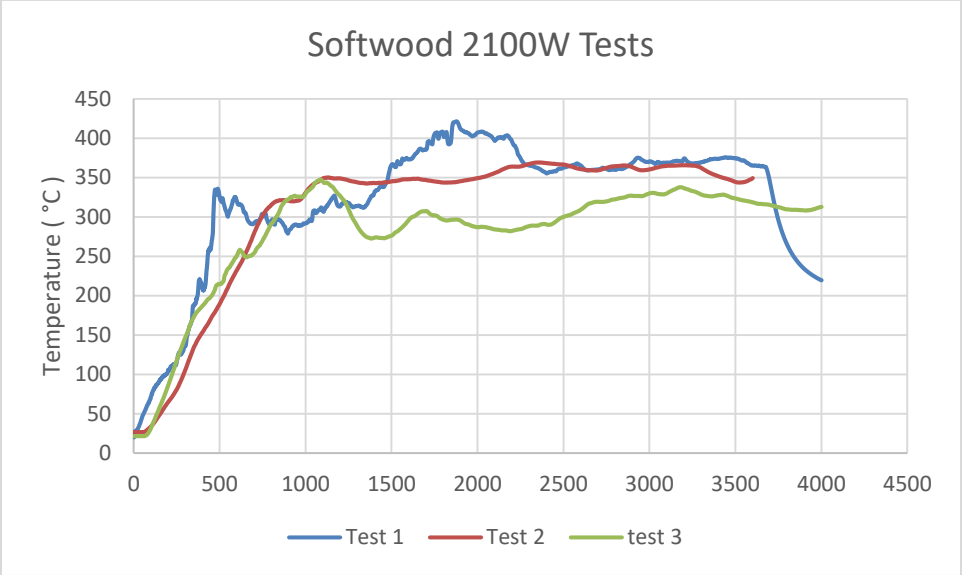

Figure B1: Softwood 2100 watt temperature profiles

Table B1: Softwood 2100 watt temperature data

Experiment #	Residence Temperature (°C)	Heating Rate (°C/min)
1	375.83	29.98
2	358.76	20.59
3	310.51	22.967
Average	348.37	24.51
Standard Deviation	33.88	4.88

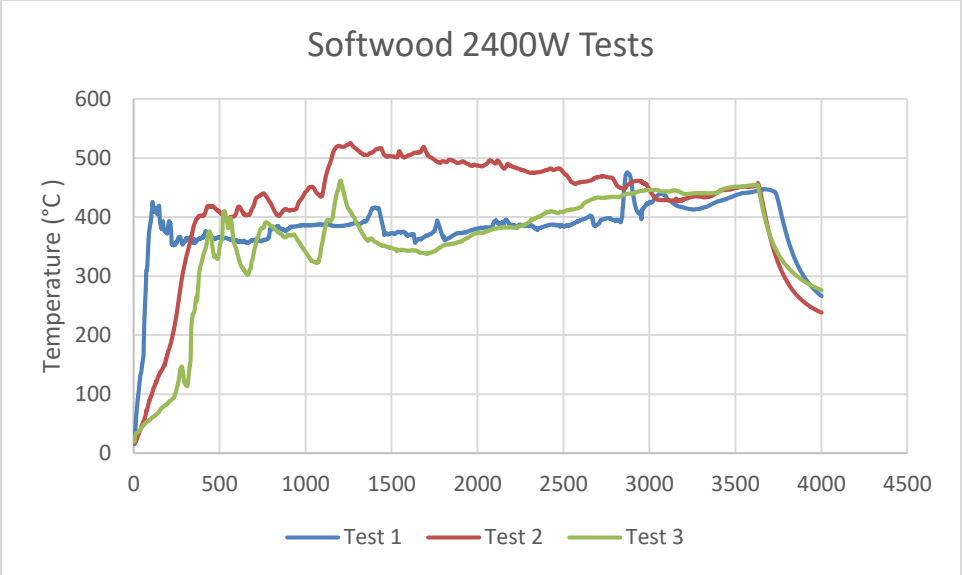

Figure B2: Softwood 2400 watt temperature profiles

Table B2: Softwood 2100 watt temperature data

Experiment #	Residence Temperature (°C)	Heating Rate (°C/min)
1	403.36	34.01
2	462.67	39.15
3	416.32	32.187
Average	427.45	35.12
Standard Deviation	31.18	3.61

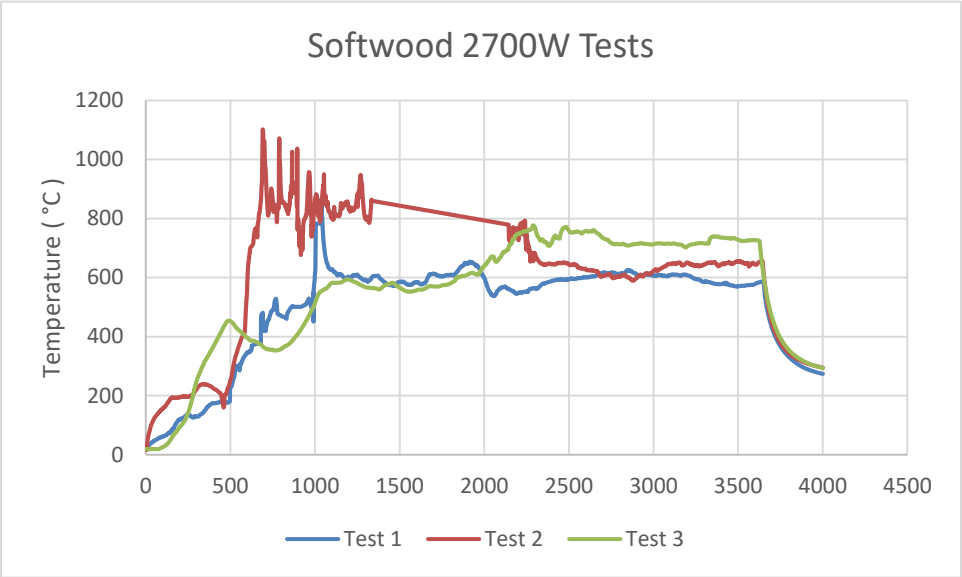

Figure B3: Softwood 2700 watt temperature profiles

Table B3: Softwood 2700 watt temperature data

Experiment #	Residence Temperature (°C)	Heating Rate (°C/min)
1	594.09	32.79
2	673.83	57.95
3	711.44	37.652
Average	659.79	42.79
Standard Deviation	59.92	13.34

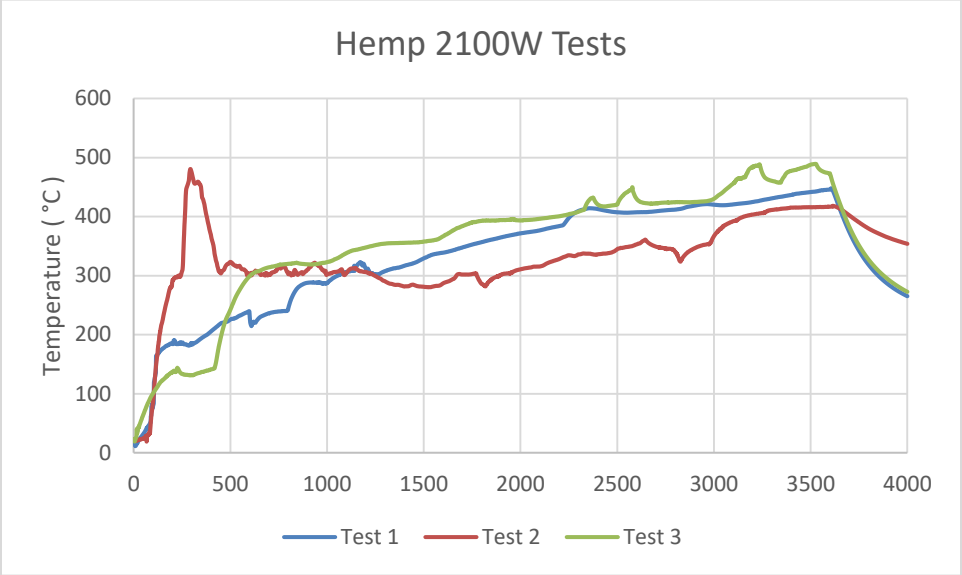

Figure B4: Hemp 2100 watt temperature profile

Table B4: Hemp 2100 watt temperature data

Experiment #	Residence Temperature (°C)	Heating Rate (°C/min)
1	408.35	20.89
2	356.26	27.72
3	431.84	27.61
Average	398.82	25.41
Standard Deviation	38.68	3.91

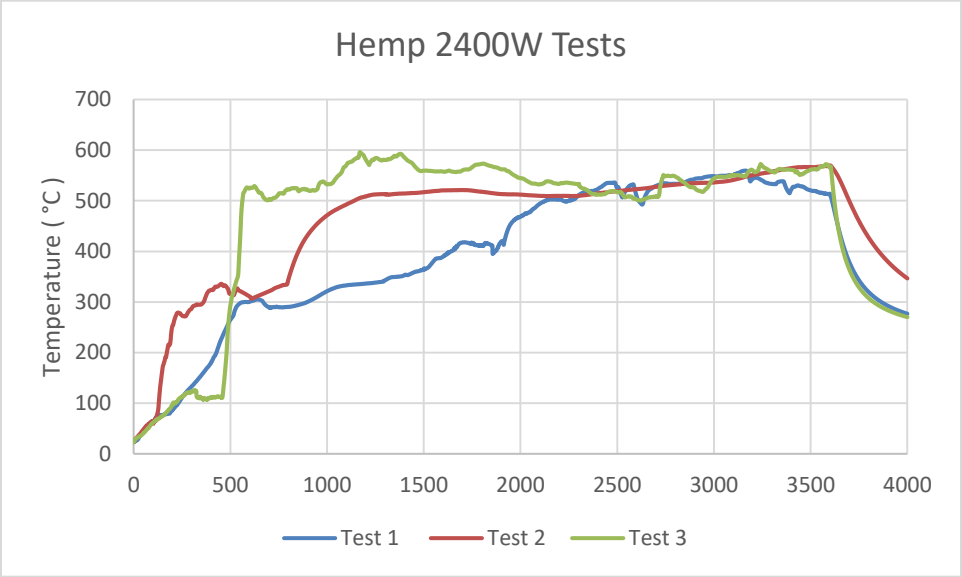

Figure B5: Hemp 2400 watt temperature profiles

Table B5: Hemp 2400 watt temperature data

Experiment #	Residence Temperature (°C)	Heating Rate (°C/min)
1	514.29	27.737
2	531.41	28.741
3	540.33	50.139
Average	528.68	35.539
Standard Deviation	13.23	12.65

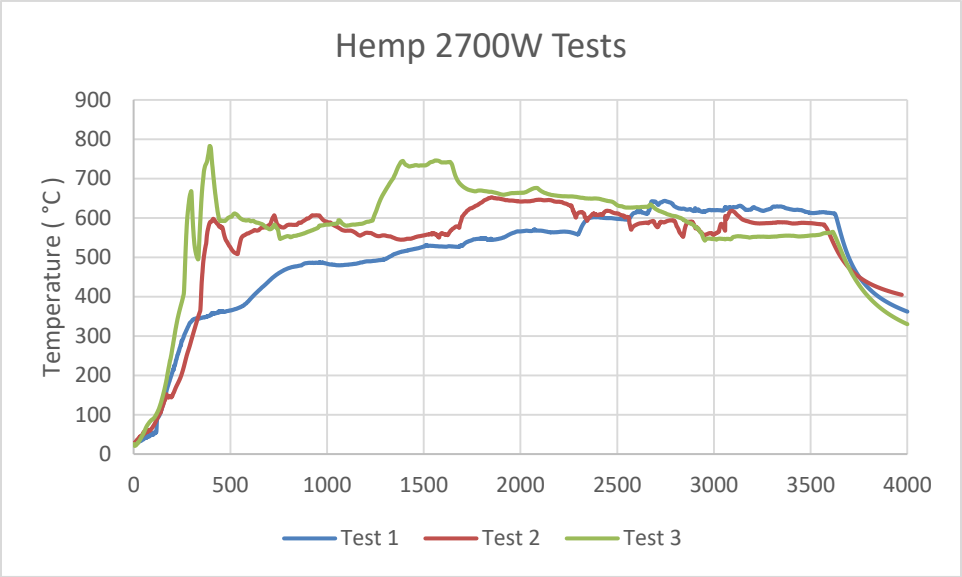

Figure B6: Hemp 2700 watt temperature profiles

Table B6: Hemp 2700 watt temperature data

Experiment #	Residence Temperature (°C)	Heating Rate (°C/min)
1	601.19	36.817
2	603.75	53.808
3	607.77	56.811
Average	604.23	49.15
Standard Deviation	3.32	10.78

Appendix C: Scanning Electron Microscopy Images

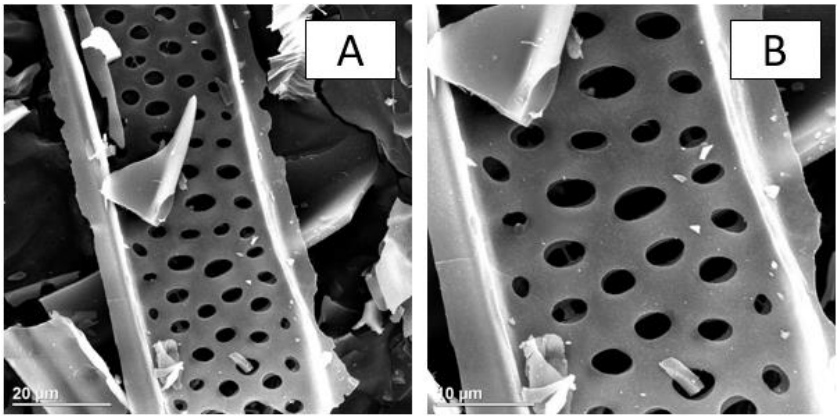

Figure C1: Hemp biochar produced at 2100 watts. SEM images - 1000x (A), 2000x (B)

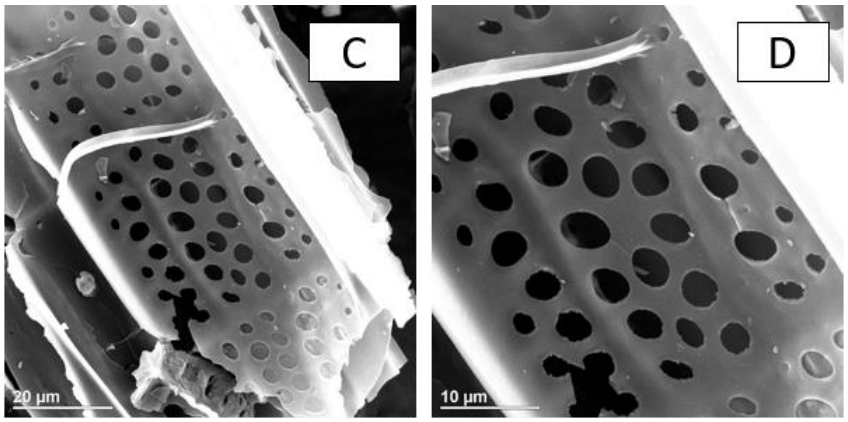

Figure C2: Hemp biochar produced at 2400 watts. SEM images - 1000x (C), 2000x (D)

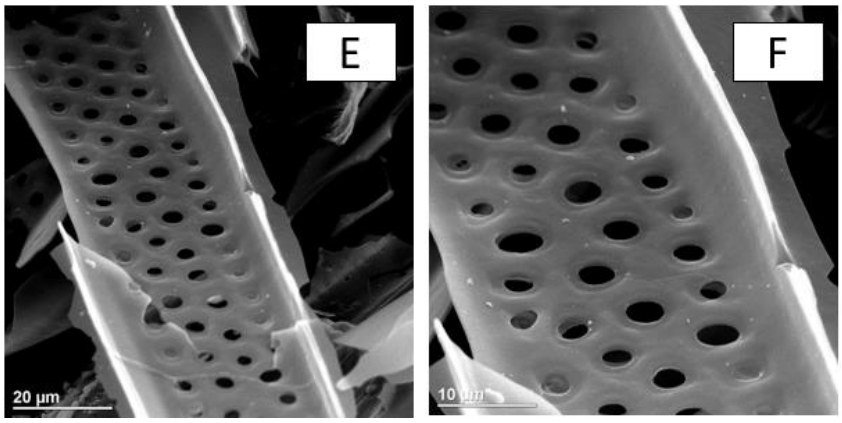

Figure C3: Hemp biochar produced at 2700 watts. SEM images - 1000x (E), 2000x (F)

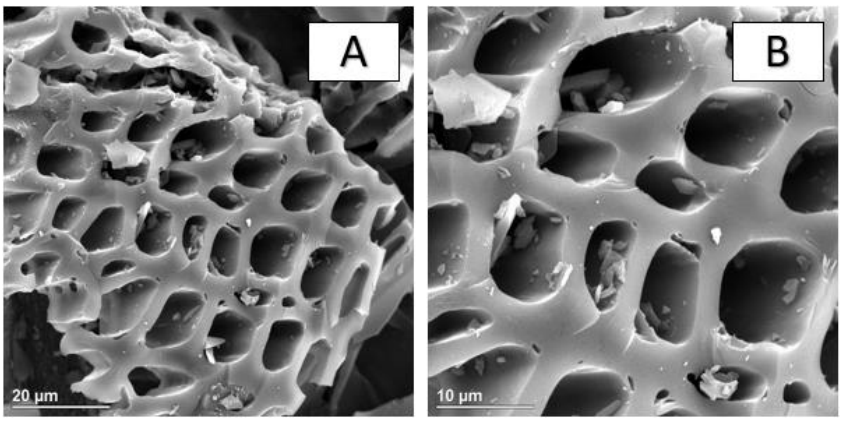

Figure C4: Softwood biochar produced at 2100 watts. SEM images - 1000x (A), 2000x (B)

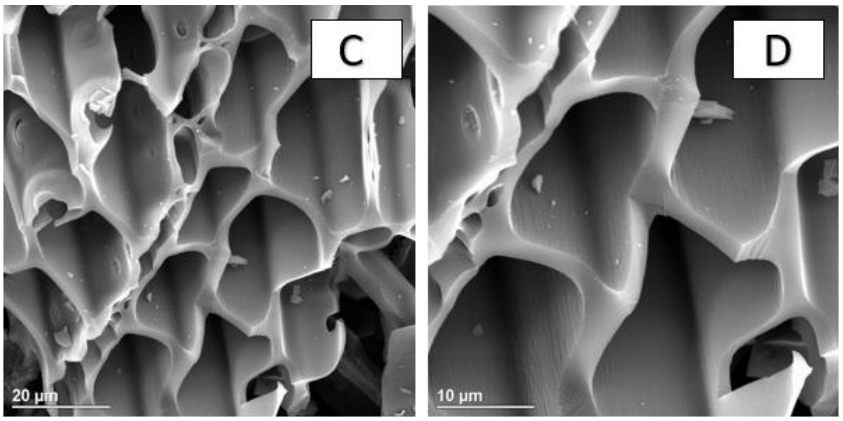

Figure C5: Softwood biochar produced at 2400 watts. SEM images - 1000x (C), 2000x (D)

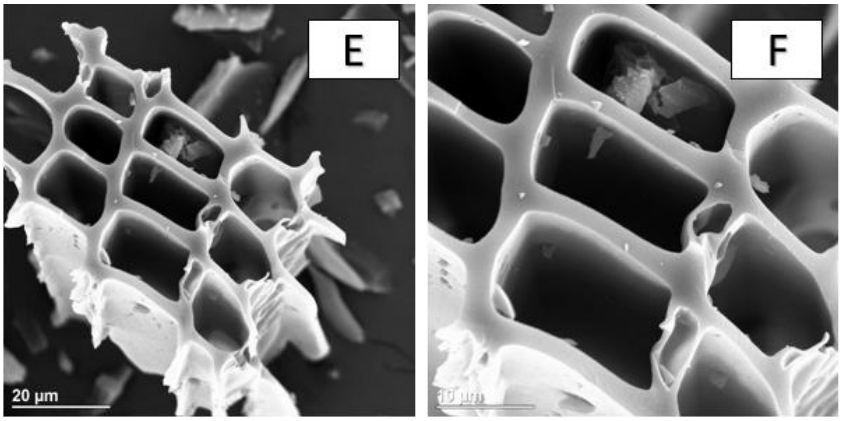

Figure C6: Softwood biochar produced at 2700 watts. SEM images - 1000x (E), 2000x (F)

Appendix D: Matlab Homogenization Code

```
%%Solved ABAQUS RVE point stress, strains, and integration point
volumes
%%imported through ABAQUS2Matlab app

i = 1; %% Looping interval

StressVol = 0; %Homogenization stress component
StrainVol = 0; % Homogenization strain component
Volume = 180*20*5; %Total volume of RVE model
Stressmtx=cell2mat(SP); %Importing RVE stresses
Strainmtx=cell2mat(EP); %Importing RVE strains
S11 = Stressmtx(:,3); %Choosing correct stresses
E11 = Strainmtx(:,3); %Choosing correct strains
a = length(Stressmtx);
IVOL = 6.6667; %Ivol same across matrix


while i < length(S11) %While loop performing homogenization
calculations
    StressVol = StressVol + (S11(i)*IVOL);
    StrainVol = StrainVol + (E11(i)*IVOL);
    i = i+1;
end

STR11 = StressVol/Volume %Final effective stress calculation
Eps11 = StrainVol/Volume %Final effective strain calculation

MOD11 = STR11/Eps11 %Homogenized composite modulus calculation
```

Curriculum Vitae

Name: Chase Alexander-John Wallace

Education: University of New Brunswick. B.Sc. Mechanical Engineering (2012 – 2017)

Publications:

1. Wallace, C.A., Saha, G.C., Afzal, M.T., Lloyd, A. (2019). Experimental and computational modeling of effective flexural/tensile properties of microwave pyrolysis biochar reinforced GFRP biocomposites, *Composites Part B: Engineering*, Under Review, 39 pages.

2. Wallace, C.A., Afzal, M.T., Saha, G.C. (2019). Effect of feedstock and microwave pyrolysis temperature on physio-chemical and nano-scale mechanical properties of biochar, *Bioresource Technology*, Submitted, 27 pages.

3. Wallace, C.A., Saha, G.C., Afzal, M.T. (2018). Experimental modeling of microwave-pyrolysis-biochar reinforced GFRP biocomposites, *26^{th} International Conference on Composites/Nano Engineering* (ICCE-26), Two-page Paper, July 15-21, Paris, France.

Conference Presentations:

1. Wallace, C.A., Saha, G.C., Afzal, M.T. *Experimental Modeling of Microwave-pyrolysis-biochar Reinforced GFRP Biocomposites.* University of New Brunswick Graduate Research Conference. (2018).

2. Wallace, C.A., Saha, G.C., Afzal, M.T. *Experimental Modeling of Microwave-pyrolysis-biochar Reinforced GFRP Biocomposites.* Atlantic Biorefinery Conference. (2018).